NONLINEAR OPTICS: MATERIALS, FUNDAMENTALS, AND APPLICATIONS

N00014-92-J-1373

Sponsored by
Air Force Office of Scientific Research
Air Force Phillips Laboratory
Defense Advance Research Projects Agency
National Science Foundation
Office of Naval Research
Strategic Defense Initiative Organization

For
Optical Society of America
IEEE/Lasers and Electro-Optics Society

POSTDEADLINE PAPERS

AUGUST 17-21, 1992
LAHAINA, MAUI, HAWAII

NONLINEAR OPTICS: Materials, Fundamentals, and Applications
Maui, Hawaii

August 17-21, 1992

Postdeadline Papers

MC5 has been withdrawn and the following paper will be presented in this time slot.

PD1 8:10pm Subpicosecond time resolved four-wave mixing spectroscopy in heteroepitaxial ZnSe thin layers, K. Takeuchi, T. Saiki, M. Kuwata-Gonokami, University of Tokyo, Japan. Resonant enhancement and quantum interference of heavy- and light-hole excitons in heteroepitaxial ZnSe thin layers are observed using picosecond and sub-picosecond time resolved four-wave mixing.

MD Poster Session I
9:05pm-10:30pm

Nonlinear Materials Postdeadline Papers

PD2 Anisotropic two-photon transition in GaAs/AlGaAs multiple quantum well waveguides, C.C. Yang, Pennsylvania State University, A. Villeneuve, G. I. Stegeman, CREOL, University of Central Florida, Cheng-Hui Lin, Hao-Hsiung Lin, National Taiwan University, Taiwan. The wavelength dependence of the two-photon absorption coefficients and nonlinear refractive-indices in the TE and TM modes of GaAs/AlGaAs multiple quantum well channel waveguides are measured.

PD3 Two picosecond, narrow-band, tunable, optical parametric systems using BBO and LBO, J.Y. Zhang, Georgia Southern University, H. T. Zhou, J. Y. Huang, Y. Ron Shen, University of California, Berkeley, C. Chen, Chinese Academy of Sciences, Peoples Republic of China. We report the operation of two picosecond, narrow-band, broadly tunable optical parametric systems using BBO and LBO. The tuning range can be extended from mid-IR to UV with sum and difference frequency generation.

PD4 Second generation in an optically active liquid: experimental observation of a fourth-order optical nonlinearity due to molecular chirality, A.V.Dubrovskii, N.I.Koroteev, A. P. Shkurinov, Moscow State University, Russia. Molesular left-right asymetry is an origin of non-vanishing even order optical nonlinear susceptibilities of non-racemic solutions of chiral molecules. Though second harmonic generation (SHG) due to quadratic dipolar nonlinearity is still symmetry forbidden in optically active liquids yet we have succeeded in experimental observation, fo the first time, of noncolli-near SHG due to five-mixing process according to a scheme 2w=3w-w, governed by a fourth order susceptibility tensor X(4)D (2w;w,w,w,-w), SH signal

is found to be well collimated and quasi phase-matched, it shows theoretically predicted polarization, spectral and temporal properties.

Photorefractives Postdeadline Paper

PD5 Optical image recognition system implemented with a 3-D memory disk, Demetri Psaltis, Hsin-Yu Li, Yong Qiao, Kevin Curtis, California Institute of Technology. We discuss the use of photorefractive crystals and photopolymers for constructing 3-D disks, and describe the implementation of a face recognizer using the 3-D disk.

NLO Organics Postdeadline Paper

PD6 Phase-matched second-harmonic generation in waveguides of polymeric Langmuir-Blodgett films, Koen Clays, Thomas L. Penner, Nancy J. Armstrong, Douglas R. Robello, Eastman Kodak Company. Based on the linear and nonlinear optical properties of all-polymeric langmuir-Blodgett films, the Cerenkov-type phasematching scheme was used for efficient second-harmonic generation.

PD7 Fluence dependent dynamics observed in the resonant third-order optical response of C60 and C70 films, S.R.Flom, J.R.Lindle, R.G.S. Pong, F. J. Bartoli, Z, H, Kafafi, U. S. Naval Research Laboratory. Fluence dependent decay dynamics are observed for ps DFWM experiments in C60 and C70 films 597 and 675 nm.

TuD Poster Session II
9:10pm-10:30pm

Fundamentals Postdeadline Paper

PD8 Temporal modulation of spatial optical solitons: a variational approach, Humberto Michinel, Raul de la Fuente, Jesus Linares, Universidade de Santiago de Compostela, Spain. A variational method is used to describe the behaviour of pulsed soliton beams in a nonlinear KERR-type medium. The results are compared with numerical simulations.

PD9 Measurements of light-scattering noise during two-wave mixing in a Kerr medium, R. Pizzoferrato, U. Zammit, M. Marinelli,Il Universita di Roma "Tor Vergata", Italy, R. McGraw, D. Rogovin, Rockwell International Science Center. Measurements of light-scattering noise during two-wave mixing in a Kerr medium

are reported. Excellent agreement with theory is obtained using the stochastic noise model.

PD10 Excess noise introduced by beam propagation through an atomic vapor, Martti Kauranen, Alenxander L. Gaeta, William V. Davis, Robert W. Boyd, University of Rochester. Two-beam-coupling gain experienced by the vacuum sidebands of a saturating laser beam gives rise to amplification of the fluctuations of the beam above the shot noise level as the beam propagates through an atomic vapor.

Techniques Postdeadline paper:

PD11 A novel approach to all-optical switching based on second-order nonlinearities, Gaetano Assanto, George I. Stegeman, Mansoor Sheik-Bahae, Eric VanStryland, CREOL, University of Central Florida. Some unique features inherent to the large nonlinear phase shift obtained from cascaded second-order processes can be exploited for efficient all-optical switching with powers in the 10's of Watt range.

PD12 Multilayer, nonlinear ARROW waveguides for surface emitted sum-frequency mixing, R. Normandin, H. Dai, S. Janz, A. Delage, J. Brown, F. Chatenoud, National Research Council, Canada. We report the first demonstration of a multilayered core ARROW type waveguide for nonlinear harmonic generation. High surface emission efficiencies were obtained in the multilayer ARROW core while simultaneously keeping optimum antiresonant conditions.

Phase Conjugation Postdeadline Papers:

PD13 Energy scaling of SBS phase conjugate mirrors to 4J, Metin S. Mangir, David A. Rockwell, Hughes Research Laboratory. A two-cell SBS oscillator-amplifier phase conjugator experiment with 4.5K, 35 ns FWHM pulses at 1.053 um, and a computer model are descibed. We obtained excellent near- and far-field conjugation fidelity even with beams having a spatially nonuniform intensity and phase aberration.

PD14 Vector versus scalar theory for the double phase conjugate mirror, Kenneth D. Shaw, U.S. Air Force Phillips Laboratory. The question of whether or not the double phase conjugate mirror functions as a photorefractive oscillator is investigated in the context of a full vectorial treatment starting from Maxwell's equations, and differences in the operatoin of the device for TE and TM polarization are discussed.

WA5 has been withdrawn and the following paper will be presented in this time slot:

9:30am
PD15 Crosstalk and error probability in counter-beam lambda-multiplexed digital holograms, A. Yariv, California Institute of Technology, Lance Glasser, Defense Advanced Research Projects Agency, George Rakuljic, Victor Leyva, Accuwave. The crosstalk and error probability in lamda-multiplexed counter-propagating holograms are evaluated. The crosstalk is also measured and compared with the theory in a LiNbO3 multi (N = 20) lambda hologram.

WE Poster Session III
9:10pm-10:30pm

NLO Materials Postdeadline Paper:

PD16 Modal growth of SHG in doped silica thin film waveguides, W. Roc White, U.S.Air Force Academy, John J. Kester, Skip C. Pribyl, Frank J. Seiler Research Laboratory. Frequency doubling of 1064 nm laser light is observed in Ge-doped SiO2 thin film waveguides.SHG growth is examined as a function of input polarization and waveguiding modes.

Subpicosecond time resolved four-wave mixing spectroscopy in heteroepitaxial ZnSe thin layers

K. Takeuchi, T.Saiki,and M. Kuwata-Gonokami

Department of Applied Physics, Faculty of Engineering, University of Tokyo,
7-3-1, Hongo, Bunkyo-ku, Tokyo 113, Japan
Telophone 81-3-3812-2111 ext. 6837

The successful demonstration of laser oscillation using ZnSe based materials [1] makes it more realistic to expand the optoelectronics into the blue region. To construct the optoelectronics system in blue region, we need efficient nonlinear materials which can work in this wavelength. Recently, we observed a very large third order optical nonlinearity at the exciton resonance in ZnSe films [2]. Ema et al. demonstrated all optical serial to parallel conversion up to sub-Tbit/sec using this material [3]. Thus the ZnSe based materials are strong candidates for the nonlinear optical devices in blue region. To know the dynamics of excitons is essential to examine the applicability of the materials to ultrafast optical devices. In this report, we discuss the dynamics and enhanced nonlinearity of excitons in heteroepitaxial ZnSe thin layers by picosecond and femtosecond time resolved four-wave mixing spectroscopy.

We use ZnSe layers with thickness about 50nm on [100] oriented GaAs substrate grown by MBE. At low temperature, the valence band splits into a heavy- and a light-hole bands, because of the biaxial strain caused by the difference in thermal expansion coefficient [4]. Heavy-hole exciton and light-hole exciton are clearly observed in the reflection spectrum as shown in the inset of Fig.2. At temperature lower than 10K, the splitting energy is about 12meV. We apply four-wave mixing (FWM) spectroscopy in reflection geometry at 10K,with picosecond and subpicosecond pulses. For picosecond pulses, we use a tunable dye laser synchronously pumped by third harmonics of a CW mode-locked YLF laser. The pulse duration is 2.5ps and the spectral width is 0.7meV. We use second harmonics of CW mode-locked Ti-sapphire laser (Coherent Mira 900) as a subpicosecond light source. The pulse duration is about 100fs and the spectral width is 13meV.

Figure 1 shows the plot of FWM signal at zero delay time as a function of incident photon energy with picosecond pulses. The FWM signal shows strong enhancement at heavy- and light-hole exciton resonances. In subpicosecond experiment, we tune the laser frequency to cover the both excitons. The spectrum is shown as a dotted curve in the inset of Fig.2. We kept the pulse energy as low as 10pJ to avoid the higher order effects. We record the diffracted intensity by changing the time delay between two excitation pulses. The dephasing time of excitons, T_2 ,

determines the FWM signal decay time, τ. τ is $T_2/2$ in a homogeneously broadened system and τ is $T_2/4$ in an inhomogeneously broadened system [5]. So from the experimental value of τ (2.4 ps), we find T_2 is in the range as $0.9meV<1/T_2<1.7meV$. We can also estimate T_2 by fitting the reflection spectrum with calculated curve of various dephasing time of excitons. We find that the best fit value of $1/T_2$ is 1.3meV, taking into account the spatial dispersion of excitons. This is in the range obtained by FWM experiment.

The modulation period, 350fs, is exactly equal to the time $h/\Delta E$, where ΔE is the splitting energy between heavy and light hole excitons. Now we consider two models which can explain the beat. One is the tree level model as shown in Fig.3(a). In this model, the short pulse excitation causes the coherent superposition of two excited states which induces the beating macroscopic polarization. The other is the model which has two independent oscillators as shown in Fig.3(b). In this model, the short optical pulse excitation starts the two oscillators with slightly different frequencies. The total polarization also beats. We can find the clear difference between two models in the modulation depth of the FWM signal. From the third order perturbational calculation [6], the model of Fig.3(a) gives the modulation depth of 100%. But modulation depth is smaller and depends on the dephasing time in the model of Fig.3(b). The maximum modulation depth is only 14% under the condition of $0.9meV<1/T_2<1.7meV$. Figure 2 shows the modulation depth of about 60%. Thus we can conclude that we can apply the first model to our experiment and the observed beat is caused by the quantum interference of heavy- and light-hole excitons.

We examine the temporal and spectral responses of time resolved four wave mixing signal in ZnSe ultrathin layers. We observe giant excitonic enhancement of third order nonlinearity and quantum interference of heavy- and light-hole excitons in this system.

The authors thank Drs. K.Ohkawa and T.Mitsuyu of Matsushita Electric Industrial Co. Ltd. for providing us the ZnSe sample and fruitful discussion. This work is supported by Grant-in Aid for Science research and technology by Ministry of Education.

References

[1] M.A.Haase, J.Qiu, J.M.DePuydt, and H.Cheng, Appl. Phys. Lett. 59, 1272 (1991)

[2] T.Saiki, K.Takeuchi, M.Kuwata-Gonokami, K.Ohkawa, and T.Mitsuyu, Appl. Phys. Lett. 60, 192 (1992)

[3] K.Ema, M.Kuwata-Gonokami, and F.Shimizu, Appl. Phys. Lett. 59, 2799 (1991)

[4] K.Ohkawa, T.Mitsuyu and O.Yamazaki, Phys. Rev. B 38, 12465 (1988)

[5] T.Yajima and Y.Taira, J. Phys. Soc. Jpn. 47, 1620 (1979)

[6] K.Leo, E.O.Gobel, T.C.Damen, J.Shah, S.Schmitt-Rink and W.Schafer, J.F.Muller, K.Kohler and G.Ganser, Phys. Rev, B44, 5726 (1991) and references therein.

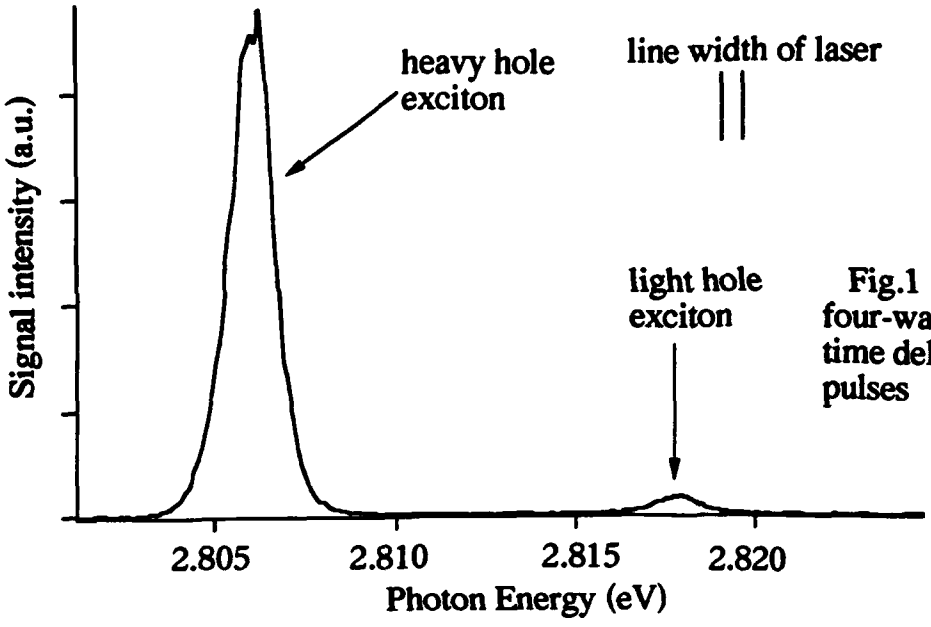

Fig.1 Resonance profile of four-wave mixing signal at zero time delay measured with 2.5ps pulses

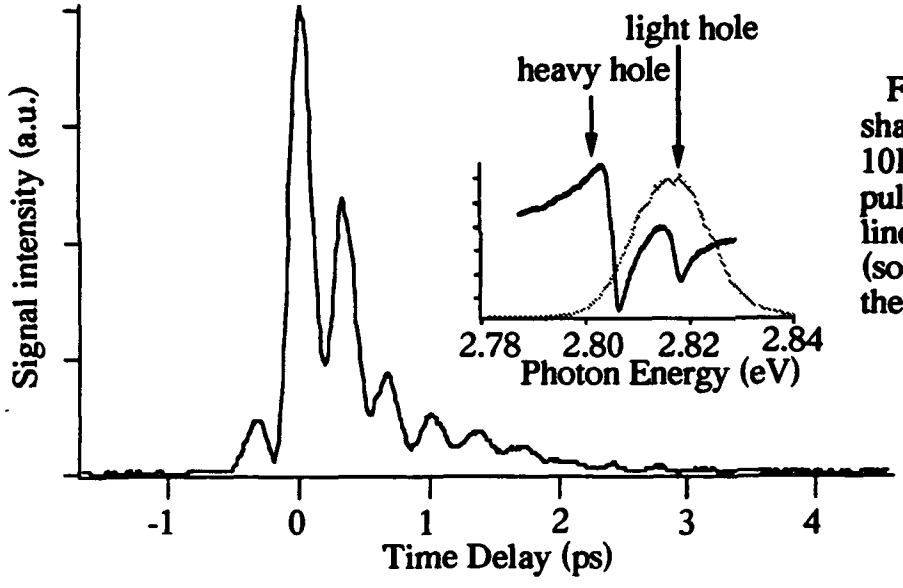

Fig.2 Four -wave mixing line shape for 50nm ZnSe layers at 10K measured with 100fsec pulses. The inset shows the linear reflection spectrum (solid line) and the spectrum of the incident pulses (dotted line)

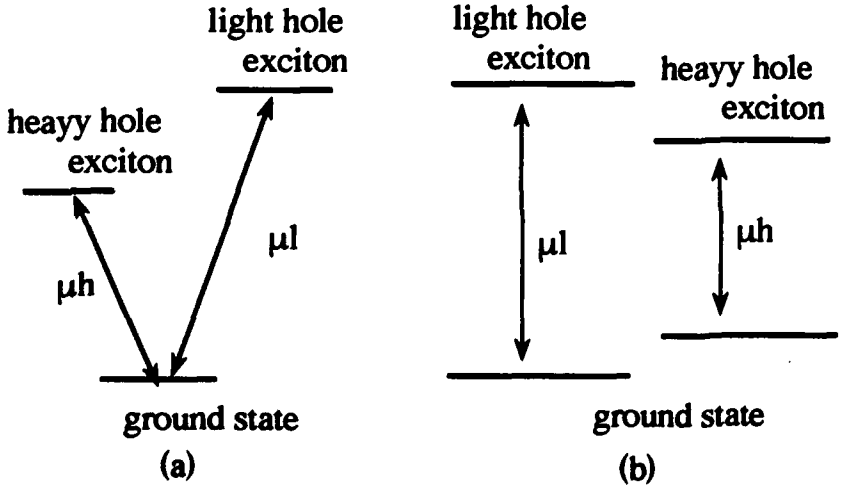

Fig.3 (a) Three level model
(b) Independent two levels model

Anisotropic Two-Photon Transition in GaAs/AlGaAs Multiple Quantum Well Waveguides

C. C. Yang
Department of Electrical and Computer Engineering
The Pennsylvania State University
University Park, PA 16802 U.S.A.

A. Villeneuve and G. I. Stegeman
CREOL, University of Central Florida
Orlando, FL 32826 U.S.A.

Cheng-Hui Lin and Hao-Hsiung Lin
Department of Electrical Engineering
National Taiwan University
Taipei, Taiwan, R.O.C.

Two-photon transitions near the absorption edge in a multiple quantum well (MQW) structure are important because, on one hand, they provide information about the energy states involved in the forbidden direct transitions[1] and, on the other hand, the induced Kerr-like optical nonlinearity has potential for ultrafast nonlinear switching applications[2]. In this paper, we report the first direct measurements of the two-photon absorption coefficient β_2 and nonlinear refractive-index n_2 in GaAs/AlGaAs MQW channel waveguides from 1490 to 1660 nm. We observed significant differences between TE and TM modes for both β_2 and n_2.

The ridge-loaded channel waveguides include a guiding layer, consisting of 85 periods of 70 Å GaAs wells and 100 Å $Al_{0.25}Ga_{0.75}As$ barriers, sandwiched by $Al_{0.25}Ga_{0.75}As$ cladding layers. The samples were made by the MBE technique. The ridge width of the waveguide used to obtain the following results is 5.5 μm. Two samples from the same wafer but with different etching depths and different lengths (one at 1.5 cm and the other one at 0.67 cm) were used. The results from the two samples are consistent. For the β_2 measurement, the inverse transmission from a color center laser was recorded. For the n_2 measurement, the self-phase modulation of the transmitted signals was analyzed by a spectrum analyzer. Numerical simulations were conducted for calibrating the data.

The results of β_2 are shown in Figs. 1 and 2 for TE and TM modes, respectively. The β_2 values in the TE mode show smooth variation with

wavelength; however, those in the TM mode illustrate two features in the measurement wavelength range. The smooth variation of β_2 in the TE

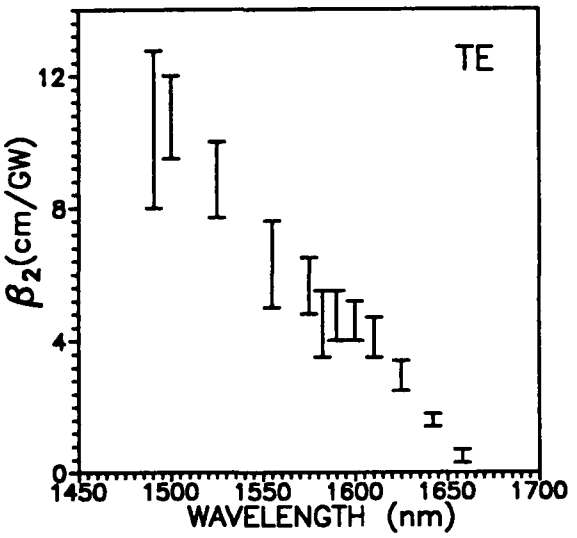

Fig. 1 β_2 values in TE mode.

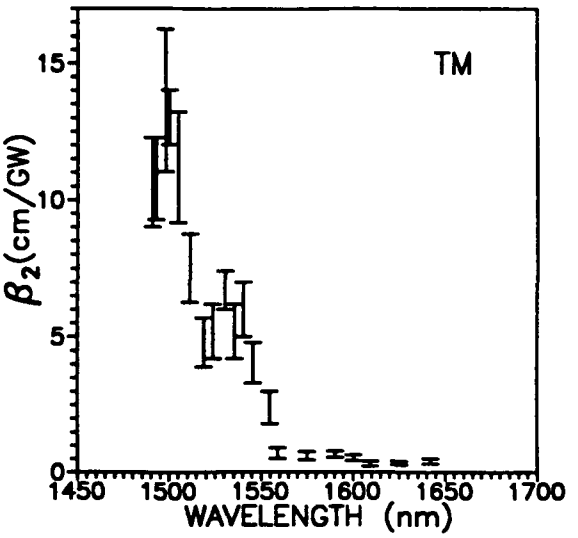

Fig. 2 β_2 values in TM mode.

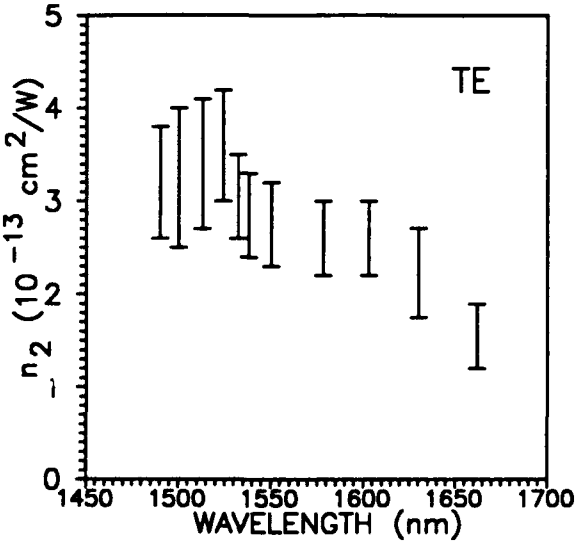

Fig. 3 n_2 values in TE mode.

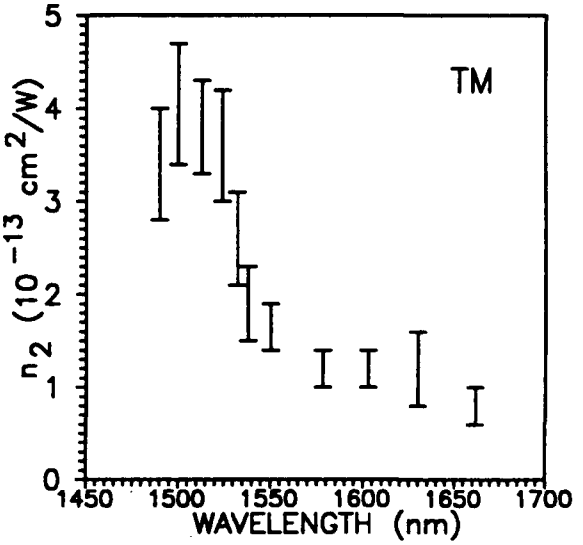

Fig. 4 n_2 values in TM mode.

mode is similar to that of a bulk material, as expected. The H1-C1(2P) exciton at the absorption edge (1640 nm) does not appear as a clear feature in our measurements[1]. The two features of β_2 in the TM mode correspond to the 1S excitons associated with the L2-C1 (at 1540 nm) and

L1-C2 (at 1500 nm) transitions[1]. The different β_2 variation in the TE and TM modes leads to a different n_2 dependence on wavelength, as shown in Figs. 3 and 4. The n_2 value in the TE mode is always larger than that in the TM mode for wavelengths longer than 1525 nm where n_2 in the TM mode almost reaches a maximum. The maximum ratio of n_2 between the two modes is larger than 2. However, the maximum n_2 for the TM mode (near 1500 nm) is higher than that for the TE mode (near 1525 nm). The large error bars basically come from the uncertainty of the linear loss coefficients in the waveguides. The nonlinear anisotropy in a MQW waveguide has potential applications to nonlinear polarization switching. The difference in n_2 between TE and TM modes will enhance the nonlinear polarization rotation along the waveguide. However, the understanding of this nonlinear polarization rotation also depends on measurements of the cross-polarization two-photon absorption coefficients and nonlinear refractive-indices[3].

References:

1. K. Tai, A. Mysyrowicz, R. J. Fischer, R. E. Slusher, and A. Y. Cho, Phys. Rev, Lett., **62**, 1784, 1989.

2. A. Villeneuve, C. C. Yang, P. G. Wigley, G. I. Stegeman, J. S. Aitchison, and C. N. Ironside, Appl. Phys. Lett., **61**, 147, 1992.

3. M. N. Islam, C. E. Soccolich, R. E. Slusher, A. F. J. Levl, W. S. Hobson, and M. G. Young, J. Appl. Phys., **71**, 1927, 1992.

Two Picosecond, Narrow-band, Tunable, Optical Parametric Systems Using BBO and LBO

J. Y. Zhang*, H. T. Zhou, J. Y. Huang, Y. R. Shen and C. Chen**
Department of Physics, University of California, Center for Advanced Materials, Lawrence Berkeley Laboratory, Berkeley, CA 94720

* Department of Physics, Georgia Southern University, Statesboro, GA 30460
** Fujian Institute of Research on the Structure of Matter, Chinese Academy of Sciences, Fuzhou, Fujian, PRC

Abstract

We report the operation of two picosecond, narrow-band, broadly tunable optical parametric systems using BBO and LBO. The tuning range can be extended from mid-IR to UV with sum and difference frequency generation.

Summary

Picosecond coherent light sources, broadly tunable from mid-IR to UV, are most useful for spectroscopic application. We report here operation of two such systems based on optical parametric amplification and oscillation in BBO and LBO crystals together with sum and difference frequency generation in BBO, LBO, $LiNbO_3$, and $AgGaS_2$.

The first system is an optical parametric amplifier (OPA), pumped by frequency-doubled 20-ps pulses from an active/passive mode-locked Nd:YAG laser. The schematic is shown in Fig. 1. With a total 3-mJ/pulse pump energy pumping two 5x5x10-mm^3 BBO crystals, the tunable output (signal only) is in the range of 100-160 μJ/pulse. The output frequency can be angle-tuned from 0.59-2.7 μm, as depicted in Fig. 2. The output bandwidth, narrowed by the grating arrangement, is less than 0.1 nm even when it is tuned to near the degenerate point. A bandwidth as narrow as 0.02 nm can be reached at a lower pump energy. To extend the tuning range to near and mid-IR as well as UV, sum- and difference-frequency generation in various crystals are used. By mixing the tunable output from OPA with the 1.06 μm output from the Nd:YAG laser in $LiNbO_3$ and $AgGaS_2$, the difference-frequency generation can yield an output tunable from 2.5-10 μm with tens of μJ/pulse. On the other hand, SHG in BBO or LBO can

extend the tuning range down to 0.3 μm with a similar output energy. It is also possible to use the third harmonic output at 355 nm from the Nd:YAG laser to pump the OPA.[1] This will further extend the UV tuning range to about 0.2 μm.

The second system is an optical parametric oscillator (OPO) synchronously pumped by 100-ps frequency-doubled, Q-switched and mode-locked Nd:YAG laser pulse trains at 500 Hz. The schematic is shown in Fig. 3. With a pump power of 600 mW pumping a 2.5x3x15 mm^3 non-critically phase-matched LBO crystal, the signal output is around 180 mW. This denotes a conversion efficiency of 30% at the signal frequency alone. The temperature-tuning curve for the OPO is presented in Fig. 4, covering a range from 0.65 to 2.7 μm. In our present experiment, the tuning range was limited to 0.78 to 0.93 μm and 1.24 to 1.67 μm by the coating of the cavity mirrors. With the grating in the cavity, the output bandwidth is reduced to around 0.06 nm. As in the case of OPA, the tuning range of the output can be extended by sum and difference frequency generation to UV and mid-IR. The conversion efficiency of second harminic generation of the signal wave is more than 10%.

This work was supported by the director, Office of Energy Research, Office of Basic Energy Science, Material Science Division of the U.S. Department of Energy under Contract No. DE-AC03-765F00098, E.I. de Pont de Nemours & Co., and the Chinese Academy of Sciences. We also thank Fujian Castech Crystals Inc. for the supply of LBO and BBO crystals.

Reference:

1. J. Y. Huang, J. Y. Zhang, Y. R. Shen, C. Chen, and B. Wu, Appl. Phys. Lett. **57**, 1961 (1991).

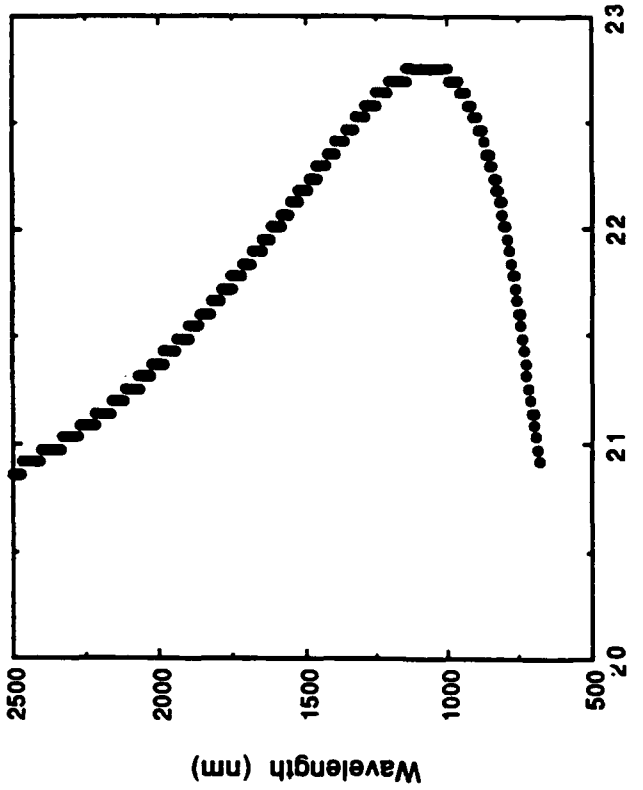

Fig.2 The tunning curve of BBO crystal.

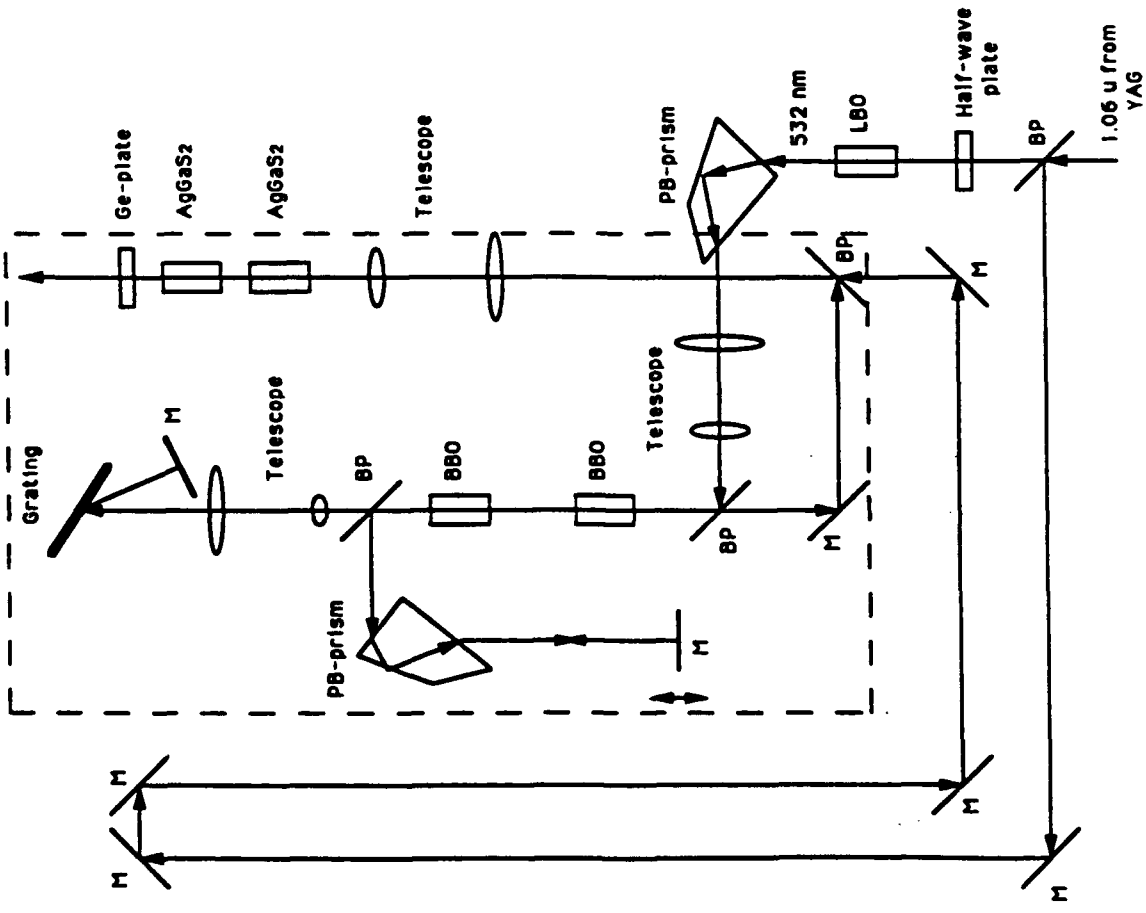

Fig. 1 The experimental arrangement of the OPA and DFG system

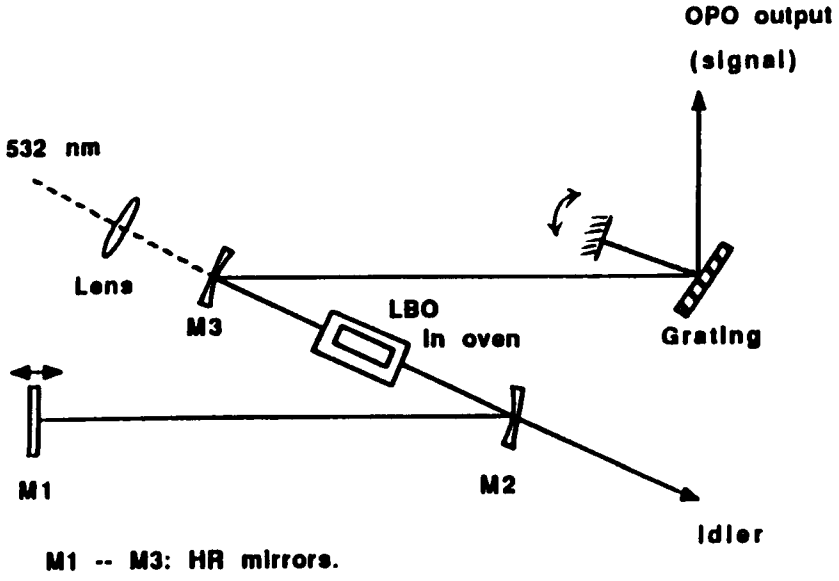

Fig.3 The optical arrangement of the OPO system

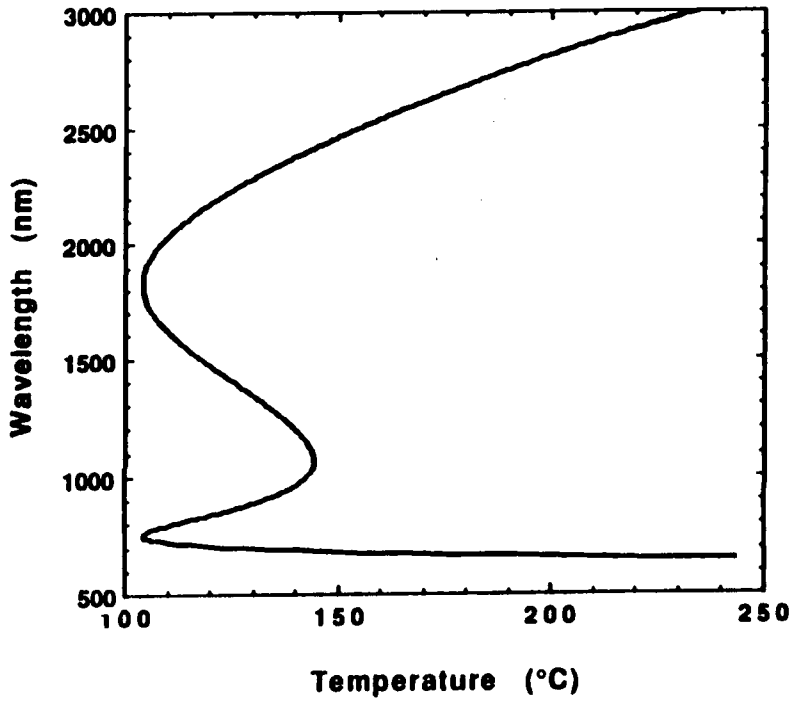

Fig.4 The tunning curve of LBO crystal.

SECOND HARMONIC GENERATION IN AN OPTICALLY ACTIVE LIQUID: EXPERIMENTAL OBSERVATION OF A FOURTH-ORDER OPTICAL NONLINEARITY DUE TO MOLECULAR CHIRALITY.

A.V.DUBROVSKII, N.I.KOROTEEV, A.P.SHKURINOV

Physics Department & International Laser Center
Moscow State University, Moscow 119899, RUSSIA

ABSTRACT

Molecular left-right asymmetry is an origin of non-vanishing even order optical nonlinear susceptibilities of non-racemic solutions of chiral molecules. Though second harmonic generation (SHG) due to quadratic dipolar nonlinearity is still symmetry forbidden in optically active liquids yet we have succeeded in experimental observation, for the first time, of noncolli-near SHG due to five-mixing process according to a scheme $2\omega = 3\omega - \omega$, governed by a fourth order susceptibility tensor $\chi^{(4)D}(2\omega; \omega, \omega, \omega, -\omega)$. SH signal is found to be well collimated and quasi phase-matched, it shows theoretically predicted polarization, spectral and temporal properties.

INTRODUCTION AND THEORY

An optically active isotropic liquid (for instance,non-racemic solution of mirror-asymmetric molecules) lacks the center of inversion and, hence, posesses nonvanishing even order dipolar nonlinear opotical susceptibilities: $\chi^{(2)D}, \chi^{(4)D}$ etc [1-3]. Optical sum-frequency generation due to $\chi^{(2)D}$ in an optically active arabinose solution was first observed by Rentzepis et al [4] in a noncollinear, phase-mismatched geometry. However, second harmonic generation (SHG) due to dipolar quadratic nonlinearity is still forbidden in such liquids because of the permutation symmetry reason [1].

Some time ago, one of us (N.I.K.)has shown that higher order nonlinearity (namely, fourth-order one) do allow the SHG process to occur in a phase-matched, noncollinear scheme [3].

This five- wave mixing process can be symbolically depicted as;

$$2\omega = \omega + \omega + \omega - \omega \qquad (1)$$

Here the latter negative ω corresponds to a second beam of fundamental frequency, crossing the first beam (three positive ω's in eq. (1)) at a phase-matching angle α (Fig.1).

The fourth- order nonlinear polarization at SH frequency, $\vec{P}^{(4)}(2\omega)$ can be written in the following form [2,3]:

$$\vec{P}^{(4)}(2\omega) = 4A^3A'\chi^{(4)D}_{31112}(2\omega;\omega,\omega,\omega,-\omega)[\vec{e}\vec{e}'^{*}](\vec{e}\vec{e}) \qquad (2)$$

Here A, A' and $\vec{e}, \vec{e}'$ are complex amplitudes and unit polarization vectors of the two beams of fundamental frequency, to be further cited as $3\vec{k}$ and $\vec{k}'$, respectively. Square brackets stand for vectorial product, and circular ones do for scalar product of vectors inside; the factor 4 reflects the partial degeneracy among frequency arguments of the fourth-order nonlinear susceptibility tensorial component $\chi^{(4)D}_{31112}(2\omega;\omega,\omega,\omega,-\omega)$.

A simple numerical estimates can be made for the peak power of the SHG signal in the approximation of the focussed gaussian beams, interacting along the phase-matching direction [2,3]:

$$P_{SH} \approx \pi w_0^2 I_{SH} \approx \frac{\pi^2 w_0^2 \omega^2}{2c^2 n} 4w_0^2 \left|\vec{P}^{(4)}(2\omega)\right|^2 \approx$$

$$\approx \frac{2^{15}\pi^4 \left|\chi^{(4)D}\right|^2 P^3 P'}{\lambda^2 c^3 n^5 w_0^4} \qquad (3)$$

Here w_0 are radii of the beam waists of focussed beams $3\vec{k}, \vec{k}'$, which are assumed to be the same for the both interacting waves, with peak powers P,P', crossing inside the liquid with

refractive index n; c is the speed of light in vacuum; A_{SH} stands for the amplitude of the second harmonic wave.

A crude estimate of $|\chi^{(4)}|$ can be done according to the following proportionality:

$$|\chi^{(4)D}| / |\chi^{(3)D}| \approx |\chi^{(3)D}| / |\chi^{(2)D}| \qquad (4)$$

an order-of-magnitude estimate for the $|\chi^{(2)}|$ can be extracted from the experiments [4]: $=10^{-9}$ esu.

That gives us the value $|\chi^{(4)D}| = 10^{-18}$ esu. Taking realistic values $w_0 = 30\,\mu m$, $P = P' = 1\,MW$ from eq.(3) we get

$$P_{SH} \approx 40\ W,$$

which corresponds, for pulses of 100 psec duration, to approximately 10^8 photons per pulse, which is more than enough for reliable detection.

EXPERIMENTAL

The experimental set-up is shown at Fig.2. It is based upon a frequency doubled,cw-pumped, acoustooptically Q-switched and mode-locked Nd:YAG laser (Yaguar), time duration of each pulse being 100 psec. Average power of the beam $3\vec{k}$ is 120 mW, and that of the beam $\vec{k}'$ is 50 mW, repetition rate, being 1 kHz. After focussing with separate lenses, the beams 3k,k' make to intersect at a phase-matching angle $\alpha = 12^\circ$ in a 2.4 M solution of d- or l-arabinose. The detection of the SH signal is performed by a fast photomultiplier tube connected with a computer-controlled single photon counting system.

In a preliminary set of experiments, we have observed a three-wave mixing process, $3\omega = \omega + 2\omega$, first reported by Rentzepis et al. [4], in 2.4M water solutions of l- and d-arabinose and α-cyclodextrine. We have succeded to see pretty intense signal at $\lambda = 365$ nm. Crude estimate of the $|\chi^{(2)}|$ value of α-cyclodextrine gives the value 4 times greater,than that of d-arabinose.

In a phase-matched configuration for the 5-wave mixing process we have observed, for the first time, second harmonic radiation with wavelength $\lambda = 266$ nm and with predicted theoretically spectral and time charact eristics (see Figs. 3,4).

A crucial test for proving the origin of this well collimated coherent signal was it's observed polarization dependence. Fig. 5 shows the variation of the SH signal from a 2.4M solution of l-arabinose with the variation of the angle φ between the polarization planes of $\vec{k}'$ and $3\vec{k}$ beams, the latter being vertically polarized and fixed. It is clearly seen from Fig.5 that $I_{SH}(\varphi)$ varies in a manner, predicted by the eq.(2).
When the equal amount of d-arabinose was added to the solution, the polarization dependence becomes flat (Fig. 5).

However, still some residual SH signal is present after the racemisationof the solution. It has coherent nature, depends on the presence of both beams. The nature of the

residual signal has to be disclosed in a separate experiment.

CONCLUSIONS

We have observed, for the first time, the five-wave mixing process of second harmonic generation, $2\omega = \omega + \omega + \omega - \omega$ in non-racemic water solutions of d- and l-arabinose. The signal demonstrates predicted polarization, spectral, spatial and time characteristics. However, the intensity of detected signal was several orders of magnitude less than estimated in the phase-matched conditions. The coherent background signal of the same frequency is observed which demonstrates no polarization dependence and insensitivity to the state of chirality of the solution.

REFERENCES

1. J.A.Giordmaine. Phys. Rev. A, 1965, v. A138, p. 1599.
2. N.I.Koroteev. In: Essays in nonlinear optics: in memoriam of Serge Akhmanov. Eds. H.Walther, N.Koroteev, M. Scully. IOP, London,1992.
3. N.I.Koroteev. Novel nonlinear optical techniques, based on optical rectification and even-order optical nonlinearities
for studying biologically important molecules. Preprint #31, Physics Department, Moscow State University, 1985.
4. P.M.Renzepis, J.A.Giordmaine, K.W.Wecht. Phys. Rev. Lett.,1966, v.16,p. 792.

1

Second Harmonic Generation in Optically Active Liquids

Five-wave mixing process

$$\vec{K}_{SH} = 3\vec{K} - \vec{K}'$$

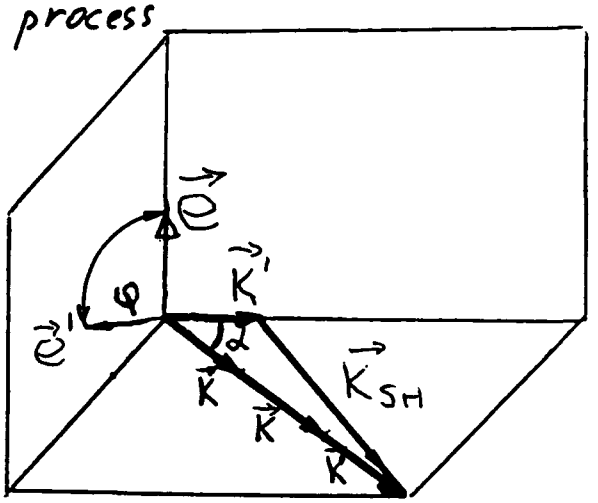

Polarization:

$$\vec{P}^{(4)D}_{SH}(2\omega) = 4\,\chi^{(4)D}_{31112}\,A^3\,A'\cdot\left[\vec{e}\,\vec{e}'^{*}\right]\left(\vec{e}\,\vec{e}\right)$$

Peak intensity $\mathcal{P}$:

$$\mathcal{P}_{SH} \sim \frac{\pi^2 w_o^2 \omega^2}{2c^2 n}\left(\sin\alpha\frac{2w_o}{tg\alpha}\right)^2 \left|\vec{e}_{SH}\vec{P}^{(4)D}(2\omega)\right|^2 \sim$$

$$\sim \frac{2^{15}\pi^4 \left|{}^{8}4\chi^{(4)D}_{31112}\right|^2 \mathcal{P}^4}{\lambda_\omega^2\, o^3\, n_{2\omega}^4\, w_o^4\, n_\omega}$$

EXPERIMENTAL SETUP FOR SECOND HARMONIC GENERATION

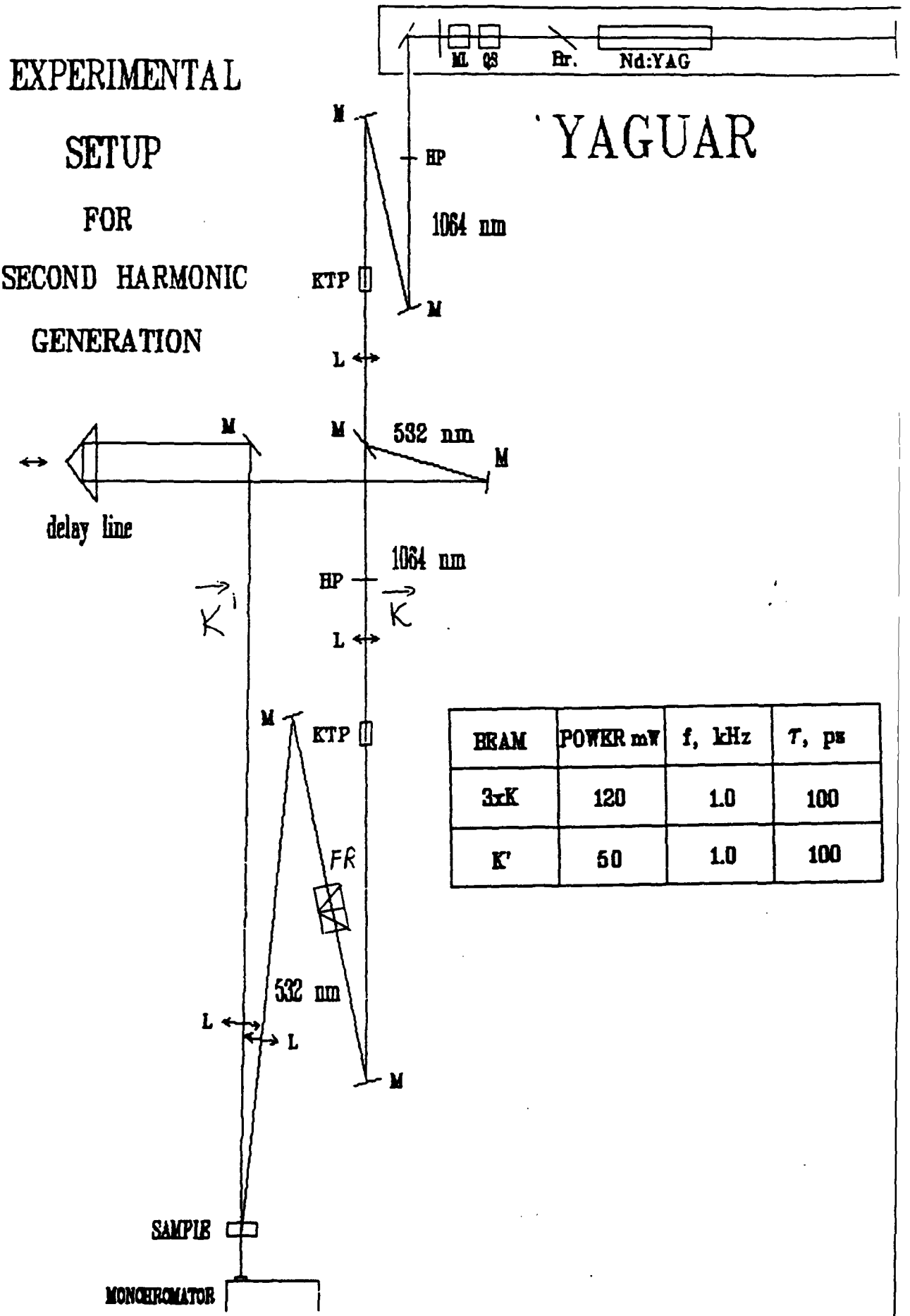

BRAM	POWER mW	f, kHz	τ, ps
3xK	120	1.0	100
K'	50	1.0	100

Five-wave mixing process PD4-7

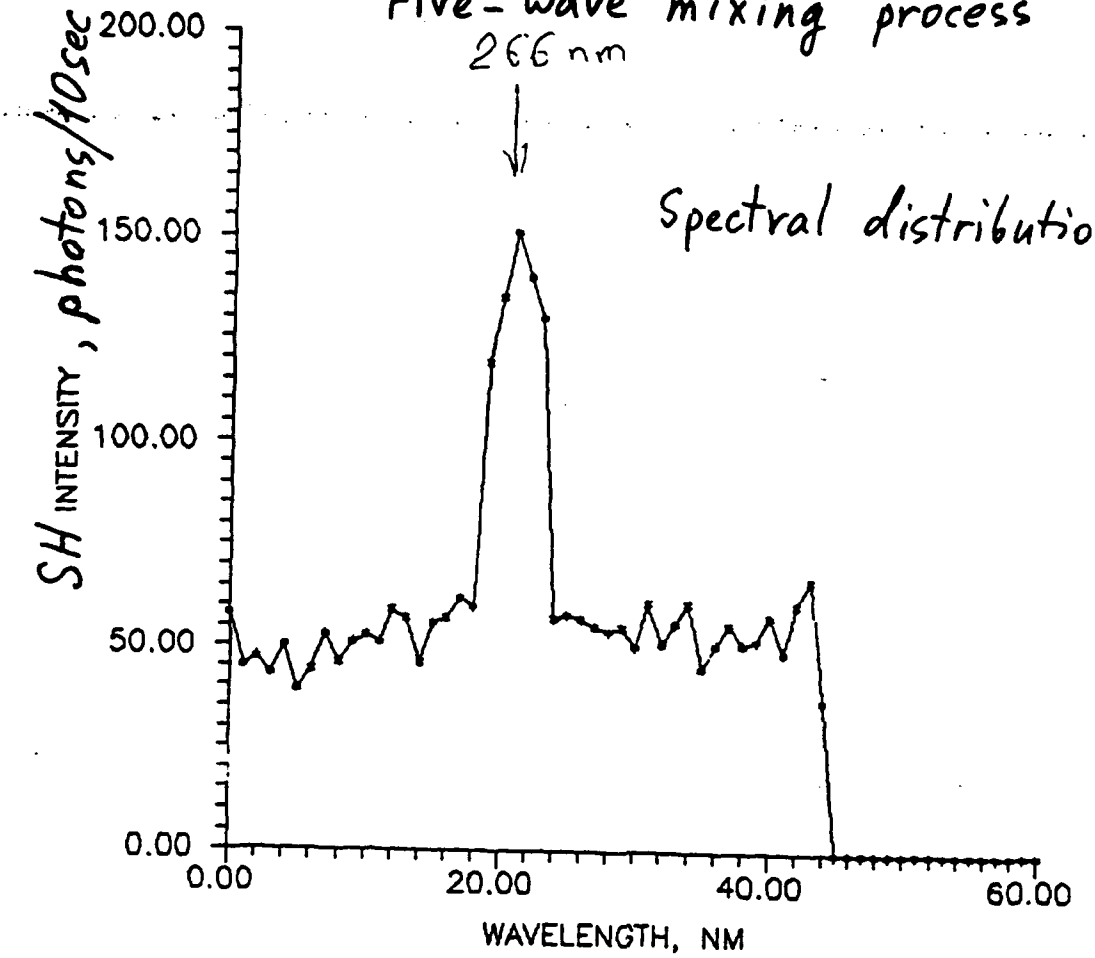

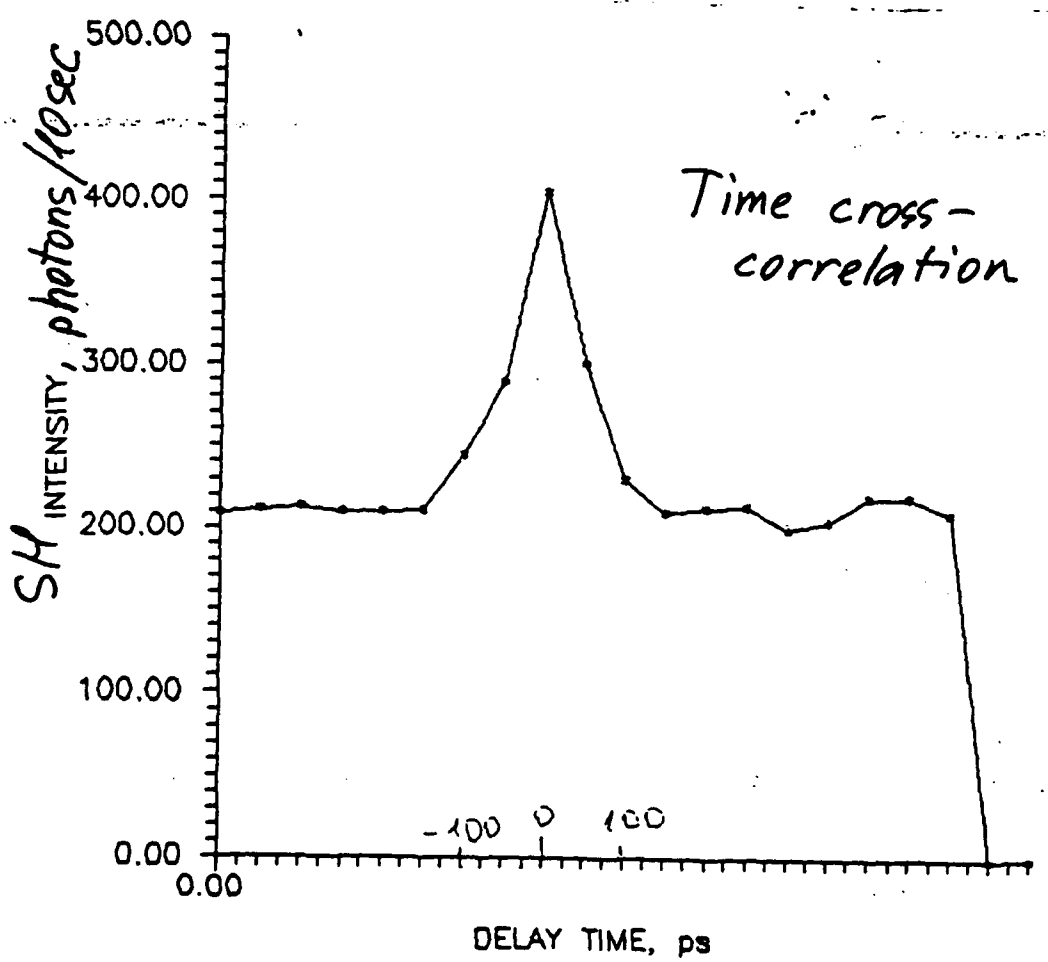

PD4-8

Experimental observation of $2\omega = \omega + \omega + \omega - \omega$

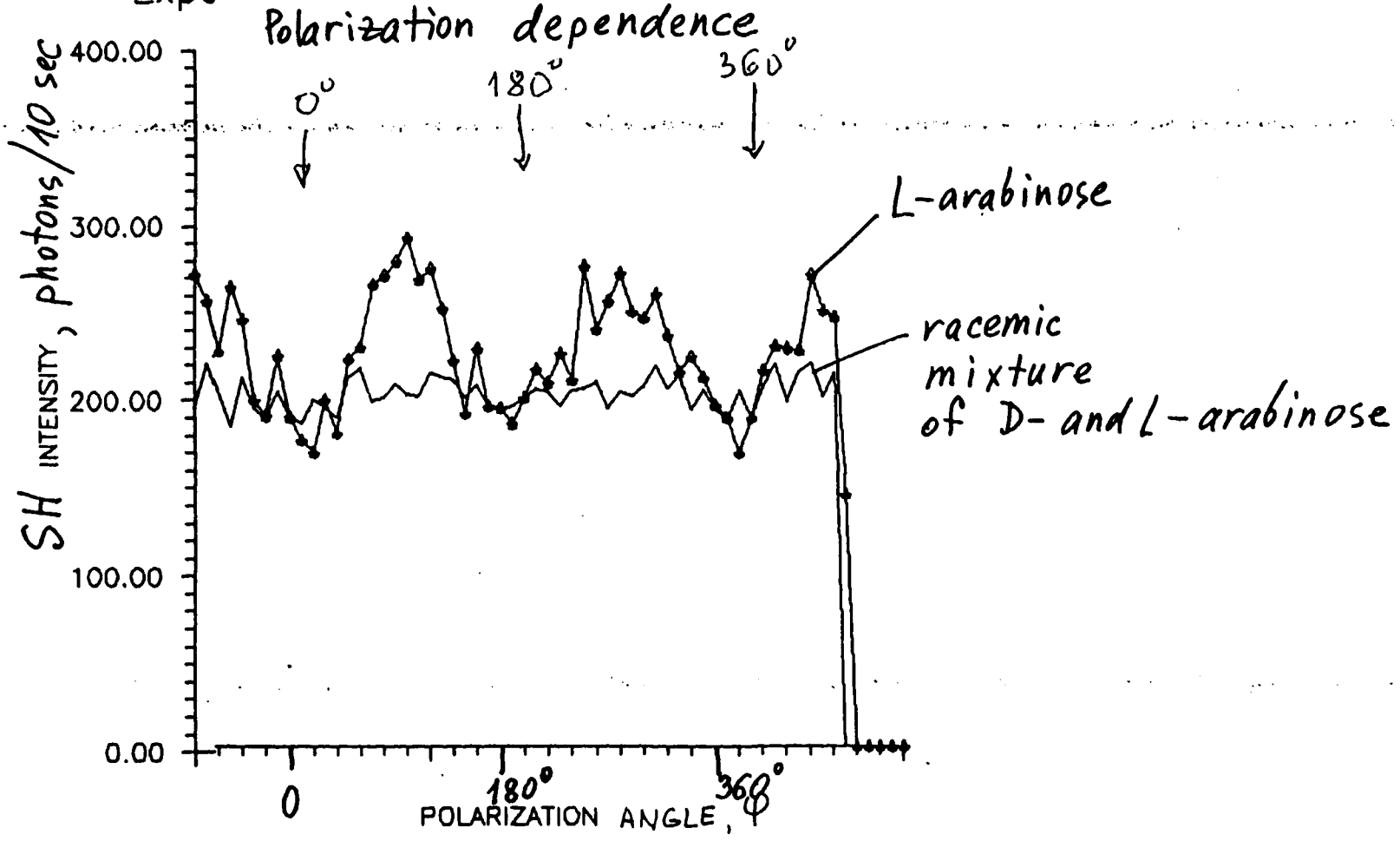

Optical Image Recognition System Implemented with a 3-D Memory Disk

Demetri Psaltis, Hsin-Yu Li, Yong Qiao, and Kevin Curtis
California Institute of Technology
Department of Electrical Engineering
Pasadena, California 91125
(818) 356-4586

SUMMARY

Holographic storage of data in 3-D media can provide high density of information storage and parallel access to the stored information. Such memories were investigated extensively in the early 60's [1,2,3,4,5] and even though these early efforts produced remarkable results they never found practical application largely because of material limitations such as low sensitivity, fanning, and hologram decay. Interest in holographic 3-D memories has been revitalized in recent years for a variety of reasons, the most significant probably being the emergence of applications, such as neural networks, machine vision, and databases, that can make use of the capabilities of holographic 3-D memories.

In this paper, we will discuss the use of non-linear optical materials for the implementation of memories and the use of such memories in image processing. Specifically, we will describe holographic 3-D disks constructed with photorefractive crystals or photopolymers. In designing a 3-D memory for holographic storage, we would like a material of optical quality that is "thick" (in the sense of recording volume holograms), has high sensitivity, and can be written on, fixed, and erased easily *in situ*. Although at present no such ideal material exists, photorefractive crystals and photopolymers fulfill many of the requirements. The applications for which they are suitable depends on their particular characteristics.

Photorefractive crystals have good optical quality, and can be grown to several millimeters to several centimeters thick. In terms of the geometry (Bragg angle selectivity) of volume holograms, they have the capacity of storing up to thousands of angular multiplexed holograms. Holograms can be recorded and erased in real time on photorefractive crystals, which makes them ideal for adaptive systems such as neural networks. Unfortunately, readout also erases the holograms. Thus when large number of exposures are required (such as in neural network learning algorithms), retaining previously recorded information on the disk becomes a problem. Although fixing techniques (such as thermal fixing) exist, they difficult to perform *in situ*, and still do not address the problem of selective erasure of information. One solution to this problem is to use a dynamic copying method [6,7]. By using periodically refreshening previously stored holograms, it is possibly to read out the information non-destructively and/or selectively erase information that has already been recorded. In addition, the dynamic copying procedure also equalizes the diffraction efficiencies of the stored holograms. Thus it is not necessary to carry out a careful exposure schedule [8] in order to obtain uniform diffraction efficiency.

Compared to most photorefractive crystals, photopolymers [9] are more sensitive to light, are much less expensive than photorefractive crystals, and have very good diffraction efficiencies. When exposed to light, photochemical reactions are induced in the photopolymers which initiate a change in the index of refraction. Once the holograms are recorded, the material is exposed to ultraviolet (UV) light to prevent further photochemical reaction. Thus photopolymers of this type are not erasable once information is recorded and fixed. However, the material is very inexpensive, can be massed produced, and is easy to fix. It is ideal for applications where the information needs to be written only once.

The theoretical upper limit on the storage density of a volume hologram is V/λ^3, where V is the volume and λ is the wavelength of light. This limit is in the order of 10^{12} samples per cm^3. However, in practical systems only 10^9–10^{10} bits per cm^3 is achievable due to the finite numerical aperture of the optical system that transfers the data into the optical system and the dynamic range of the material. For photorefractive crystals, typically approximately 10^3 holograms are superimposed in crystals with volumes of $1cm^3$, each hologram having a resolution of $10^3 \times 10^3$ pixels, giving a total memory of 10^9 bits.

In order to further increase the storage capacity of 3-D memories using these materials, it is necessary to spatially multiplex many such recording locations on a single memory. This can be most conveniently done by making the memory in the form of a disk. Different recording locations on the disk are then accessed by rotating the 3-D disk, and different holograms recorded at the same location by angle multiplexing are accessed by changing the read-out reference beam angle.

In fabricating a 3-D disk for holographic data storage, it is important that the material is uniform throughout the disk in terms of diffraction efficiency. For photopolymers (which are isotropic) the main issue is the uniformity of quality and thickness of the material. For photorefractive crystals, the problem becomes more complicated due to the anisotropic nature of photorefractive crystals. We would like to select a crystal orientation and recording geometry that maximizes the diffraction efficiency, but at the same time minimizes the *variation* of diffraction efficiency as the reference beam angle changes and the disk rotates. An analysis of the problem indicates that the for $LiNbO_3$, a good configuration is to have the c-axis of the crystal as the rotational axis, and to record reflection-type holograms. Our analysis also shows that for crystals belonging to the 4mm symmetry group (e.g., $BaTiO_3$ and SBN), there is no variation with respect to rotation angles.

As mentioned earlier, holographic data storage provides high density information storage and parallel access to the stored information. In addition, the fact that data is stored in the form of holograms makes it possible to do much of the information processing directly. We demonstrate a two-layer neural network that uses a 3-D holographic memory disk for face-recognition. The network is implemented with liquid crystal spatial light modulators for the input plane and lithium niobate photorefractive crystals for the interconnection to the first layer. The network has approximately 60,000 input units (or 'neurons'), 30 hidden units, and one output unit. The information for specifying the interconnection weight from the input layer to the hidden layer was stored holographically on one location of the 3-D disk. A 1.5 minutes video of a person (Robert) was taken, from which 180 frames were selected as the "training set". Each hidden unit was trained to respond to 6 frames. The trained network classified the rest of the training tape almost flawlessly. The system

was then tested by presenting through a TV camera real time images of Robert and other members of our group. The system almost never mis-classifies other people as Robert and exhibits remarkable tolerance to changes in aspect, illumination, and facial expression.

References

[1] P.J. Van Heerden, *Appl. Optics*, **2**, 393 (1963).

[2] K. Blotekjaer, *Appl. Optics*, **18**, 57 (1979).

[3] L.K. Anderson, *Bell Labs. Rec.*, **6**, 318 (1968).

[4] J.-P. Huignard, J.-P. Herriau, and F.. Micheron, *Appl. Phys. Lett.*, **26**, 256 (1975).

[5] L. d' Auria, et al., *Appl. Opt.*, *13*, 808 (1974).

[6] Y. Qiao, D. Psaltis, C. Gu, J. Hong, and P. Yeh, "Phase-locked sustainment of photorefractive holograms using phase conjugation," *J. Appl. Phys.*, **70**(8), 4646–4648 (1991).

[7] Y. Qiao and D. Psaltis, "Sampled Dynamic Holographic Memory," Submitted to *Opt. Lett.*

[8] D. Psaltis, D. Brady, and K. Wagner, "Adaptive Optical Networks Using Photorefractive Crystals," *Appl. Opt.*, **27**(9), 1752–1759 (1988).

[9] H.E. Zimmerman and A.M. Weber, "Photochemical rearrangement of molecules having quenchers on a chain-mechanisitic and exploratory organic-photochemistry," *J. Am. Chem. S.*, **111**(33), 995–1007 (1989).

PHASE-MATCHED SECOND-HARMONIC GENERATION IN WAVEGUIDES OF POLYMERIC LANGMUIR-BLODGETT FILMS

Koen Clays,* Thomas L. Penner, Nancy J. Armstrong, and Douglas R. Robello

Corporate Research Laboratories
Eastman Kodak Company
Rochester, New York 14650

Langmuir-Blodgett (LB) films have been fabricated from a preformed acrylate amphiphilic copolymer with nonlinear optical (NLO) active chromophores covalently attached to the polymer backbone. By alternate deposition of this NLO active polymer with a NLO passive amphiphilic polymer, high quality multilayer films have been obtained with sufficient thickness to allow waveguiding in the LB films. The observed optical attenuation is between 1 and 3 dB/cm. The linear and nonlinear optical characteristics of these films have been determined, both in transmission (or reflection) and in waveguide format. The high degree of chromophore order observed in these LB films makes this type of supramolecular structure attractive for NLO applications. Based on the observed parameters (dispersion of the refractive indices, birefringence, absorption, tilt angle of the chromophore, hyperpolarizability), the guided-mode-to-substrate-radiation-mode Cerenkov phase-matching scheme was used for efficient second-harmonic generation.

---

*present address:
Laboratory of Chemical and Biological Dynamics
University of Leuven, Belgium

Fluence Dependent Dynamics Observed in the Resonant Third-Order Optical Response of C_{60} and C_{70} Films.

Steven R. Flom, J.R.Lindle, R.G.S.Pong, F.J.Bartoli and Z.H.Kafafi
Optical Sciences Division
Naval Research Laboratory
Washington, DC 20375
{202-767-9252]

The fullerenes, C_{60} and C_{70}, are molecules whose properties have been receiving increasing attention. Their high degree of symmetry and their three dimensional π-electron systems make them intriguing candidates for their potential nonlinear optical (NLO) properties. In order to investigate the resonant third-order optical response we have performed time resolved degenerate four-wave mixing (DFWM) experiments on films of pure C_{60} and pure C_{70} at 597 and 675 nm using an amplified ps laser system. The films were made by vapor deposition and characterized by FTIR and UV-Visible absorption spectroscopies.

Table 1 summarizes the magnitude of $|\chi^{(3)}_{xxxx}|$ observed in the DFWM measurements, the absorption coefficients and the refractive indices[1], as well as the ratios of $\chi^{(3)}_{xyyx}/\chi^{(3)}_{xxxx}$ for the two compounds at the two different wavelengths. The DFWM studies show that the magnitude of the resonant nonlinear response observed in the fullerenes is comparable to the resonant response observed for polydiacetylenes[2] or phthalocyanines.[3,4] The variation of $|\chi^{(3)}_{xxxx}|$ with wavelength follows the variation of the absorption coefficient, with the implication that optical pumping mechanisms are a principle source of the nonlinear response. The unusually small values of $\chi^{(3)}_{xyyx}/\chi^{(3)}_{xxxx}$ support this premise since nonresonant electronic and nuclear contributions yield ratios ranging from 1/3 to 3/4 depending on the relative importance of the nuclear and electronic contributions.[5] Contributions of optical pumping mechanisms to $\chi^{(3)}_{xyyx}$ are determined by the time correlation function of the excited state dipole with that of the ground state.[6,7] In C_{60} (I_h symmetry point group), the correlation is zero since the degeneracies of the excited states are threefold or higher. In other words, the near spherical excitation symmetry yields an excited state with no memory of the ground state orientation. For C_{70}, the small ratio observed is consistent with an excited state that, similarly, has little orientational correlation with the ground state, despite the lower symmetry point group, D_{5h}, and the attendant doubly degenerate excited state. In either case, making the

reasonable assumption that the nuclear responses are neglible, the observed small size of the ratio yields an upper limit for the nonresonant electronic part of $\chi^{(3)}_{xxxx}$. Since $3\chi^{(3)nr}_{xyyx} = \chi^{(3)nr}_{xxxx}$ and the observed $\chi^{(3)}_{xyyx}$ has no excited state contribution the upper limit for $\chi^{(3)nr}_{xxxx}$ for C_{60} is 1.2×10^{-11} esu and 7.6×10^{-11} esu for C_{70}.

Table 1

Fullerene	λ nm	n	α $10^3 cm^{-1}$	$\chi^{(3)}_{xxxx}$ 10^{-11}esu	$\chi^{(3)}_{xyyx}/\chi^{(3)}_{xxxx}$
C_{60}	597	2.03	9.2±1.4	38±9	<0.011
	675	1.99	1.5±0.1	8.2±0.8	<0.07
C_{70}	597	2.12	48.2±0.3	210±10	<0.012
	675	2.04	8.5±3.0	64±20	<0.02

Figure 1 shows a log plot of the time dependence of the parallel polarized DFWM signal for C_{70} at 597 nm at a fluence of 6.8 mJ/cm². Two features are readily apparent; the late time signal does not return to the baseline and the signal near zero time decays rapidly. These features are observed in the dynamics of both C_{60} and C_{70} at both wavelengths. For the thicker films an acoustic response also appears in addition to the constant late time response. The presence of a response that persists much longer than the 1 ns time scale of the experiment is probably due to the triplet state; solution experiments[8–11] indicate that triplets are produced in high yield and have lifetimes on the order of microseconds.

Figure 2 shows that, at 597 nm, the early response of C_{60} depends strongly on the laser fluence. The kinetic traces in figure 2 have been normalized at the peak and the (small constant) long time signal has been subtracted. With the principle mechanism of the NLO response presumed to be optical pumping, the dynamics of the NLO response are determined by the dynamics of the excited state. The data at all fluences shown are nonexponential in qualitative agreement with the the nonexponential transient absorption data of Cheville and Halas[12]. The important feature of the data is that the overall decay becomes much more rapid as fluence increases. Figure 3 shows that the nonexponential decays observed from films of C_{70} at 597 nm are, in contrast, almost independent of the incident fluence. Since the linear absorption coefficient of C_{70} is approximately six times larger than that of C_{60} at this wavelength, it may be that the difference in the fluence dependence of the kinetics is simply related to the difference in the population density of the excited states. Indeed, when the wavelength of the laser system is changed to 675 nm,

where the absorption coefficient of C_{70} is comparable to that of C_{60} at 597 nm, the C_{70} dynamics are similar to those observed for C_{60} at 597 nm. This result is demonstrated in Figure 4 where C_{70}'s dynamics over the first 40 ps of the decay show strong dependence on the laser fluence. Similar dynamics are observed for C_{60} at 675 nm.

Nonlinear transmission experiments for C_{60} and C_{70} at the same two wavelengths demonstrate that both molecules act as reverse saturable absorbers over this wavelength region. That is, the observed transmission through the sample decreases with increasing intensity. Simulations to estimate the cross sections and population densities are underway. Preliminary results show excited state cross sections larger than those measured for the ground state and small populations of upper excited states. Our dynamic data above indicate that the apparent lifetime of the initially excited state depends on its population, changing from tens of ps at low fluence to considerably shorter at high fluence. The high fluence fast decay can be modeled by bimolecular kinetics. The shortening of the excited state lifetime is consistent with an excitonic singlet–singlet annihilation mechanism in competition with a molecular decay.

References

1. S.L.Ren, Y.Wang, A.M.Rao, E.McRae, J.M.Holden, T.Hager, K.Wang, W–T.Lee, F.Ni, J.Selegue and P.C.Ecklund, *Appl. Phys. Lett.*, **59**, 2678 (1991); S.L.Ren, K.Wang, P.Zhou, Y.Wang, A.M.Rao, M.S.Meier, J.P.Selegue and P.C.Ecklund, *Appl. Phys. Lett.*, **61**, 124 (1992).
2. G.M.Carter, M.K.Thackur, Y.J.Chen and J.V.Hryniewicz, *Appl. Phys. Lett.*, **47**, 457 (1985).
3. S.R.Flom, J.S.Shirk, J.R.Lindle, F.J.Bartoli, Z.H.Kafafi, R.G.S.Pong and A.W.Snow, *Proc. Mat. Res. Soc.*, **247**, xxx (1992).
4. M.K.Casstevens, M.Samoc, J.Pfleger and P.N.Prasad, *J. Chem. Phys.*, **92**, 2019 (1989).
5. J.Etchepare, G.Grillon, J.P.Chambaret, G.Hamoniaux and A.Orszag, *Opt. Commun.*, **63**, 329 (1987).
6. B.Meyers and R.M.Hochstrasser, *IEEE J. Quant. Electron.*, **QE22**, 1482 (1986).
7. F.W.Deeg and M.D.Fayer, *J. Chem. Phys.*, **91**, 2269 (1989).
8. M.R.Wasielewski, M.P.O'Neil, K.R.Lykke, M.J.Pellin, and D.M.Gruen, *J. Am. Chem. Soc.*, **113**, 2774 (1991).
9. J.W.Arbogast, A.P.Darmanyan, C.S.Foote, F.N.Diedrich, R.L.Whetten and Y.Rubin, *J. Phys. Chem.*, **95**, 11 (1991).
10. R.J.Sension, C.M.Phillips, A.Z.Szarka, W.J.Romanow, A.R.McGhie, J.P.McMauley,Jr., A.B.Smith III, R.M.Hochstrasser, *J. Phys. Chem.*, **95**, 6075 (1991).
11. J.W.Arbogast and C.S.Foote, *J. Am. Chem. Soc.*, **113**, 8886 (1991).
12. R.A.Cheville and N.J.Halas, Phys. Rev. B, **45**, 4548 (1992).

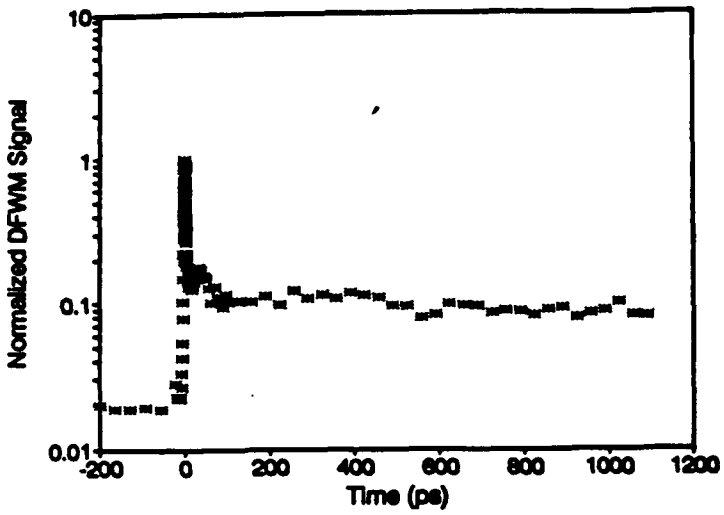

Figure 1 Time dependence of the DFWM signal measured at 597 nm and a laser fluence of 6.8 mJ/cm² for a 150 nm thick film of C_{70}.

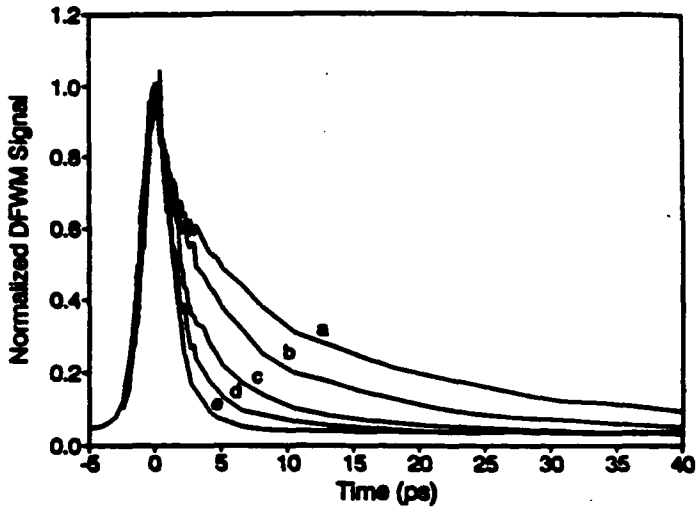

Figure 2 The early temporal response measured as a function of laser fluence for a 1200 nm thick C_{60} film. a) 0.91 b) 1.4 c) 2.4 d) 4.1 e) 11 mJ/cm² at 597 nm.

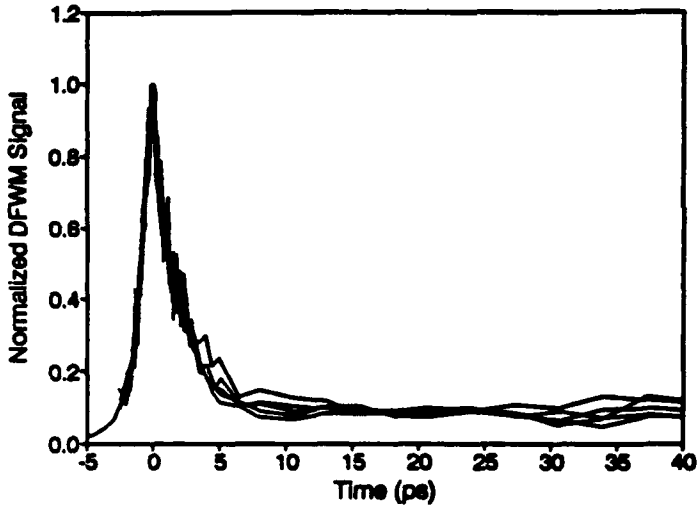

Figure 3 The early temporal response measured as a function of laser fluence for a 150 nm thick C_{70} film. a) 0.73 b) 1.5 c) 2.4 d) 4.5 e) 6.8 mJ/cm² at 597 nm.

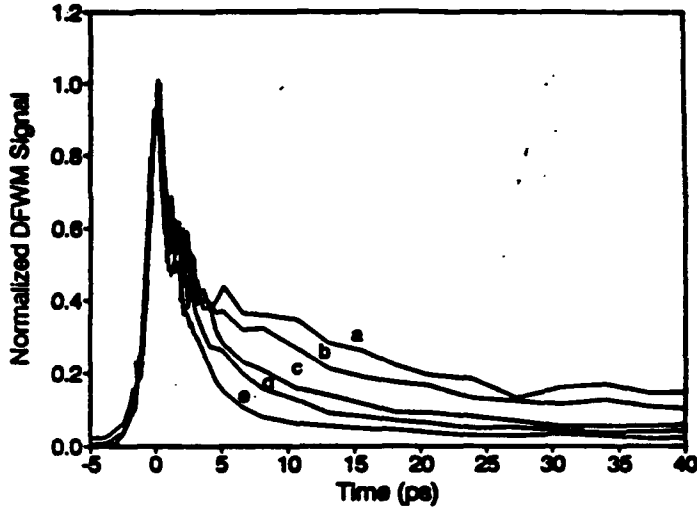

Figure 4 The early temporal response measured as a function of laser fluence for a 970 nm thick C_{70} film. a) 0.22 b) 0.33 c) 0.90 d) 1.3 e) 2.8 mJ/cm² at 675 nm.

TEMPORAL MODULATION OF SPATIAL OPTICAL SOLITONS: A VARIATIONAL APPROACH

Authors: Humberto Michinel, Raúl de la Fuente and Jesús Liñares.

Laboratorio de óptica, Facultade de Física, Universidade de Santiago de Compostela, SPAIN.

Spatial optical solitons are self-trapped optical beams that propagate without changing their spatial shape. This behaviour is caused by the competing effects of diffraction and selfocusing in a non-linear medium. Zakharov and Shabat[1] explained the connection between self-trapping and soliton theory. They also showed the complete analogy between temporal solitons, in wich the nonlinear phase modulation balances dispersion and spatial solitons in wich the non-linear index profile balances diffraction.

Comparing with temporal optical solitons, we must stress that only recently a special atention to spatial ones have been paid[2,3]. In the present work temporal effects on a pulsed ligth beam are investigated. That is, a spatial distribution of ligth with a finite-width temporal envelope. The variational results obtained[4] for temporal pulses are extended here to study pulsed beams propagation in non-linear mediums with a refractive index of the form $n = n_1 + n_2 I$ (I the intensity of the beam). It is obtained a relationship between the temporal envelope form and the evolution of the spatial beam width. The interest of these investigations arises from the potential use of these phenomena for all-optical switching and processing applications.The analisys is restricted to short distances of propagation along the z-axis. This means that dispersion effects can be neglected because the relation between the temporal widths (described by the root mean square width σ[5]) at $z=0$ and $z=z_0$ approaches to one. Let us consider a distribution of initial form:

$$\Psi(0,x,\tau) = N(\tau)\,\mathrm{sech}(x) \qquad [1]$$

with τ the reduced time and $N(\tau)$ a supergaussian temporal envelope:

$$N(\tau) = N \exp\left[-\left(\frac{\tau}{\tau_0}\right)^{2m}\right] \qquad m = 1,2,3... \qquad [2]$$

In this case, dispersion will not be considered when:

$$\frac{\sigma(z_0)}{\sigma(0)} = \left[1 + \frac{\Gamma\left(2-\frac{1}{2m}\right)}{\Gamma\left(\frac{3}{2m}\right)}\left(\frac{mz_0}{L_D}\right)^2\right]^{\frac{1}{2}} \approx 1 \Rightarrow mz_0 << L_D \qquad [3]$$

where Γ is the gamma function and L_D the dispersion length given by[5]:

$$L_D = \frac{\tau_0^2}{\beta} \quad \text{with} \quad \beta = \frac{d^2k(\omega)}{d\omega^2} \quad \text{the constant of propagation} \qquad [4]$$

In the slowly-varying envelope approximation, within the previous assumptions, the propagation equation is the non-linear Schrödinger wave equation:

$$i\frac{\partial\Psi(z,x,\tau)}{\partial z} = \alpha\frac{\partial^2\Psi(z,x,\tau)}{\partial x} + |\Psi(z,x,\tau)|^2\,\Psi(z,x,\tau) \qquad [5]$$

The reduced time τ does not appear in [5] as a variable. It only plays the role of a parameter. This is the main

consequence of neglecting dispersion.

We consider now an independent evolution model of τ=constant sections of the initial distribution [1]. Each section corresponds to a (spatial) initial value problem. The different initial conditions (determined by τ) are considered to evolve independently on each other. At a recquired distance of propagation, the temporal envelope is reconstructed using the variational results. Following this model, the variational method[4] gives the evolution of [1] as the (trial) function:

$$\Psi(z,x,\tau) = A(z,\tau)\ \mathrm{sech}\left(\frac{x}{a(z,\tau)}\right) e^{i\Phi(z,\tau)x^2} \qquad [6]$$

where the intensity is given by:

$$|A(z,\tau)|^2 = \frac{N^2(\tau)}{a(z,\tau)} \qquad [7]$$

For $1/2<N^2(t)< 1$ the corresponding initial condition preserves the soliton character. This means that the energy far from the center of the pulsed beam is asymptotically loosed by diffraction. We will investigate the evolution of the soliton part, wich is given by the condition:

$$\tau < (\ln 2)^{\frac{1}{2m}}\tau_0 = \tau_s \qquad [8]$$

The spatial width evolves oscillating between the following minimun and maximun values:

$$a_{min} = 1 \qquad [9\ a]$$

$$a_{máx} = \frac{1}{2N^2(\tau)-1} \qquad [9\ b]$$

The average value of $a_{máx}$ and a_{min} is:

$$\bar{a} = \frac{N^2(\tau)}{2N^2(\tau)-1} \qquad [10]$$

For N~1 this mean value coincides with the asymptotic soliton width predicted by inverse scattering theory[7]. However, the trial function [6] cannot describe the transition from the initial oscillatory state to an asymptoically emerging soliton and a dispersively decaying part.

The main result deduced from [9] is the existence of a temporal modulation on the spatial width. As numerical simulations show (fig 1), this modulation depends on the temporal envelope shape. This effect has been experimentally observed[6] and is now explained by this variational approach. As we are interested in spatial solitons. Thus, we calculate the energy distribution $E(x,z_0)$ for a given plane z_0 of observation as the following average over τ: .

$$E(x,z_0) = \int_0^{\tau_s} |\Psi(x,\tau,z_0)|^2\, d\tau \qquad [15]$$

where $\Psi(x,\tau,z_0)$ is given by [11]. The results plotted in figure 2 show that the square-like temporal envelope (m>>1) preserves more accurately the initial energy distribution than the gaussian temporal envelope (m=1). It is also shown that the variational result approaches to the numerical one in the square envelope limit. In this case all the initial conditions are equal to the exact solution of the equation [5]. Thus, the indepependent sections evolve without changes in their spatial shapes and there is no contribution of the difracted energy. In the gaussian limit (m=1), the difference between the numerical and the variational result is more important than in the square limit (m>>1) case. But the behaviour of the central part of the beam shows a good agreement.

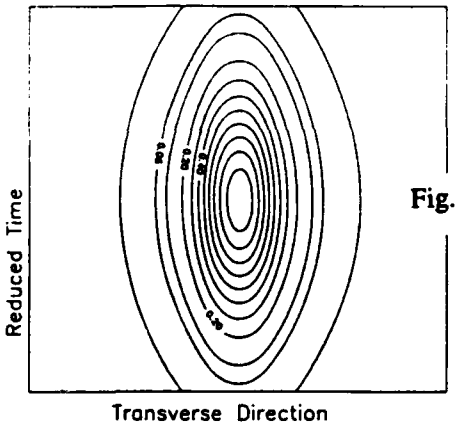

Fig. 1 a)

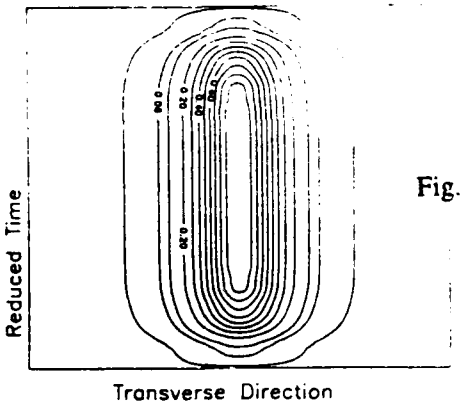

Fig. 1 b)

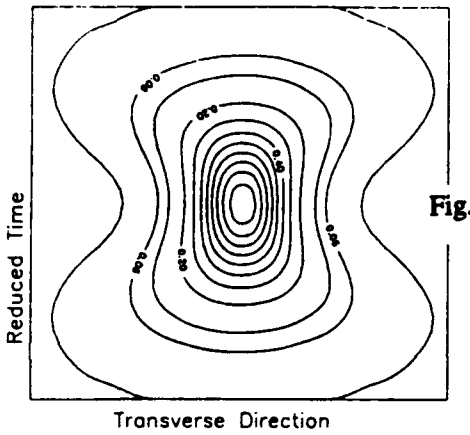

Fig. 1 c)

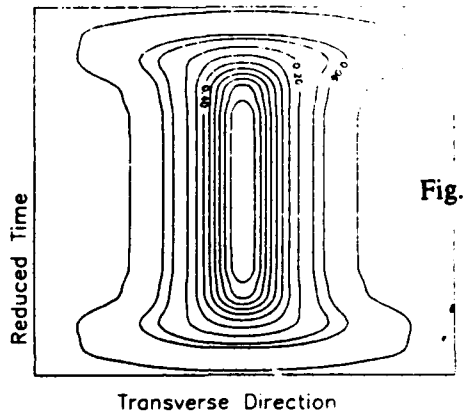

Fig. 1 d)

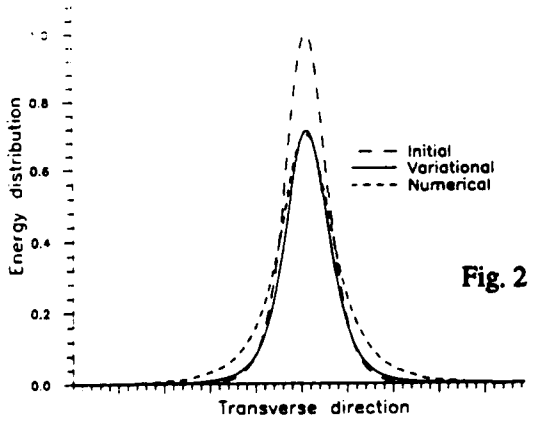

Fig. 2 a)

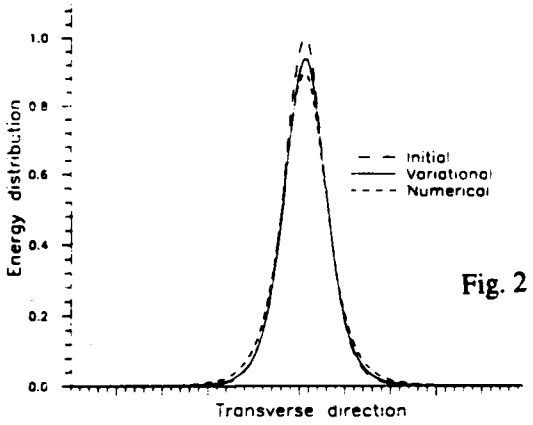

Fig. 2 b)

Fig. 1: Level plot of the intensity distribtion for different values of m and distances z_0 of propagation.

a) m=1, z_0 = 0 cm. b) m=4, z_0 = 0 cm. c) m=1, z_0 = 5cm. d) m=4, z_0 = 5cm.

Fig. 2: Normalized energy distributions along x-axis for different values of m.

a) m=1 b) m=4

Distance of propagation: 5 cm. n1: 1.6. n2: 3.0 10^{-14} cm^2/W. Wavelength: 1.064 μm. Spatial width: 60 μm.

Temporal width: 30 psec. Initial. peak power: 5.119 $10^8 W/cm^2$. Soliton peak power: 5.119 10^8 W/cm^2.

References:

(1) V.E.Zakharov, A.B. Shabat. Sov.Phys.JETP.34, 62 (1972).
(2) A.Barthelemy, S.Maneuf, C.Froehly. Opt.Comm.3, 201 (1985).
(3) J.S.Aitchison et.al. J. Opt.Soc.Am B. 6, 1290 (1991).
(4) D.Anderson. Phys. Rev. A. 6, 3135 (1983).
D.Anderson, M.Lisak, T.Reichel. J.Opt.Soc.Am.2, 207 (1988).
(5) G.P.Agrawal. "Nonlinear fiber optics".Ac.Press, N.Y. (1989).
(6) S.Maneuf, A.Barthelemy, C.Froehly. J.Optics 17, 139(1986).
(7) J.Satsuma, N.Yayima. Suppl.Prog.Theo.Pys.55, 284 (1974).

Measurements of light-scattering noise during two-wave mixing in a Kerr medium

R. Pizzoferrato, U. Zammit, and M. Marinelli

Dipartimento Ingegneria Meccanica, II Universita di Roma "Tor Vergata"
Via E. Carnevale, 00173 Rome, Italy

R. McGraw and D. Rogovin

Rockwell International Science Center
1049 Camino Dos Rios, Thousand Oaks, CA

ABSTRACT

Measurements of light-scattering noise during two-wave mixing in a Kerr medium are reported. Excellent agreement with theory is obtained using the stochastic noise model.

SUMMARY

In this paper we report the first measurements of noise during two-wave mixing in a Kerr medium and demonstrate excellent agreement with theoretical predictions for thermal light-scattering noise (1). Measurements of gain and noise were made using liquid suspensions of polytetrafluoroethylene (PTFE) shaped microparticles as artificial Kerr media. Particles are ellipsoidal in shape (the dimensions are 0.4μm x 0.2μm x 0.2μm) and the particle polarizability tensor has corresponding symmetry. The particle suspensions are highly monodisperse and interparticle interactions are negligible even at relatively high volume fractions (0.1 - 2%). In the present experiments we typically used a 1% volume fraction of PTFE particles suspended in a 65/35 water/glycerol host-liquid mixture. This mixture was chosen because it matches the average value of the particle refractive index $n_0 = 1.376$ thus minimizing the importance of light-scattering fluctuations due to the isotropic part of the particle polarizability (2,3).

The pump and the probe waves for the nondegenerate two-wave mixing experiments are provided by splitting the 514-nm TEM_{00} output of a cw Argon-ion laser into a 1W- power pump beam and a 50mW probe beam. The two beams eventually intersect within the sample at an angle of 5 degrees. The beam waist size is about 100 μm and the interaction length is 0.1 cm. Before entering the sample, the polarization direction of the pump beam is rotated perpendicular to that of the probe so that only the orientational particle gratings are generated in the suspension by the beam interference pattern. The angular frequency shift Ω required for the nondegenerate beam configuration is provided to the pump beam by a mirror that is mounted to a piezoelectric transducer (PZT). A triangular 8-Hz high-voltage wave is fed through the PZT so as to produce a periodic linear displacement of the mirror with constant, sign-inverting speed. The consequent square-wave-like angular frequency shift can be varied by either changing the amplitude or the frequency of the mirror displacement. The periodic intensity gain of the probe beam is revealed by a low-noise photodiode. A polarizer is placed before the photodiode to remove the polarized component of the pump light scattered into the probe beam by the isotropic particle fluctuations. After a low-pass electrical amplification (-3dB at 3kHz), the photodiode output is fed both into a digital oscilloscope and into a 12-bit, PC-interfaced spectrum analyzer. For each value of the frequency shift, the average value of the intensity gain was obtained by a digital average on the oscilloscope while the spectral properties of the gain fluctuations were monitored on the spectrum analyzer.

Figure 1a shows the experimental results for the probe intensity gain and noise fluctuations. Pump light intensity in the sample was approximately 10 kW/cm^2 while the transmitted probe power in the absence of the pump beam was 50mW. The vertical bars report the transmitted probe-beam power in Watts as a function of the nondimensional frequency shift $\Omega\tau$, where $\tau = \tau_R = 8.9$ ms is the orientational response time as determined through independent measurements (10). Each vertical bar is centered on the average value of the transmitted power and the bar length reports the root-mean-square (RMS) value of the noise fluctuations on the same scale. RMS noise fluctuations are also shown in the figure on an expanded scale for clarity (full circles) and were obtained by integration of the noise power spectrum over a collection bandwidth of 60 Hz. The smooth curve is a fit to the data using $\sigma(P_2) = C\,[1 + (\Omega\tau)^2]^{-1/2}$, which is the form expect-

ed from the theory, which will be described.

For comparison with experiment, calculations were made using the stochastic noise model (1). The one adjustable parameter in the theory is the Kerr coefficient, and this is obtained here from a fit to the gain curve, not to the noise. The gain curve shown in Fig. 1b was obtained using $\varepsilon_2 = 3.6 \times 10^{-7}$ cm^3/erg, in reasonable agreement with the estimate for this quantity obtained from previous nonlinear optics measurements (2,3): $\varepsilon_2 = 2.5 \times 10^{-7}$ cm^3/erg. Remaining conditions used in the calculations are the same as those described above for the experiment. The simulation proceeds by the following steps: (1) A value for $\Omega\tau$ is selected and the theory of Ref. 1, which is based on the fluctuation-dissipation theorem, is used to obtain the mean and variance for the noise amplitude fluctuations over the measurement bandwidth B = 60 Hz. (2) The Maxwell equations governing beam propagation with noise are solved to obtain the transmitted field $E_2(L)$ and corresponding amplified signal power $P_2(L)$. Steps 1 and 2 are repeated on the order of a thousand times to obtain a good statistical sampling of the noise over the full $\Omega\tau$ range of interest. Results of the calculation are shown in Fig. 2b. Note that both the experimental and theoretical gain profiles follow frequency dispersion curves characteristic of the Debye relaxation model (2,3). More importantly, there is excellent agreement between theory and experiment in regard to the RMS values of the noise fluctuations, including their dependence on frequency shift. This agreement is remarkable, in view of the lack of adjustable parameters in the theory.

1. R. McGraw, J. Opt. Soc. Am. B9, 98 (1992).

2. R. Pizzoferrato, D. Rogovin, and J. Scholl, Opt. Lett. 16, 297 (1991).

3. M. De Spirito, R. Pizzoferrato, M. Marinelli, U. Zammit, D. Rogovin, R. McGraw, and J. Scholl, Opt. Lett. 16, 120 (1991).

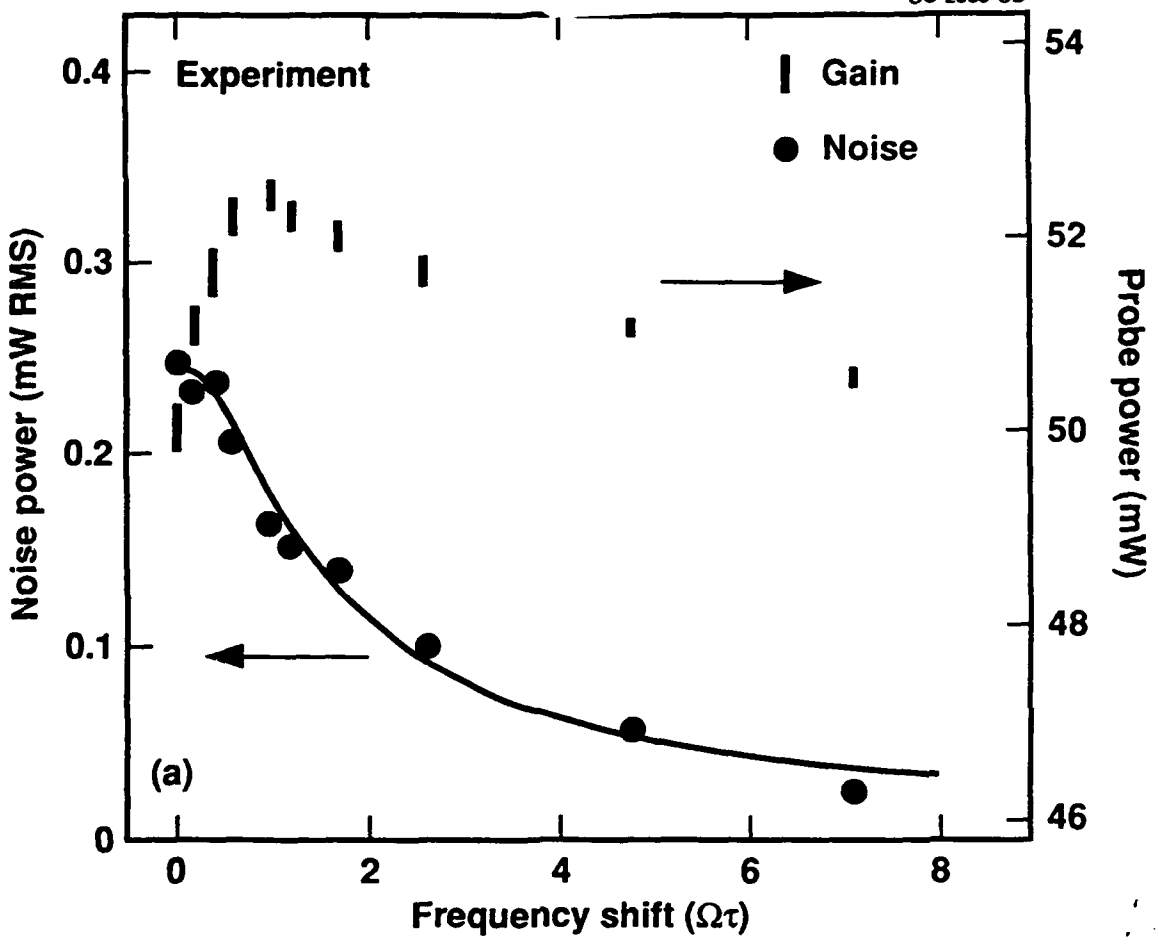
Experiment
Gain
Noise
(a)
Noise power (mW RMS)
Probe power (mW)
Frequency shift (Ωτ)
0
0.1
0.2
0.3
0.4
46
48
50
52
54
0
2
4
6
8

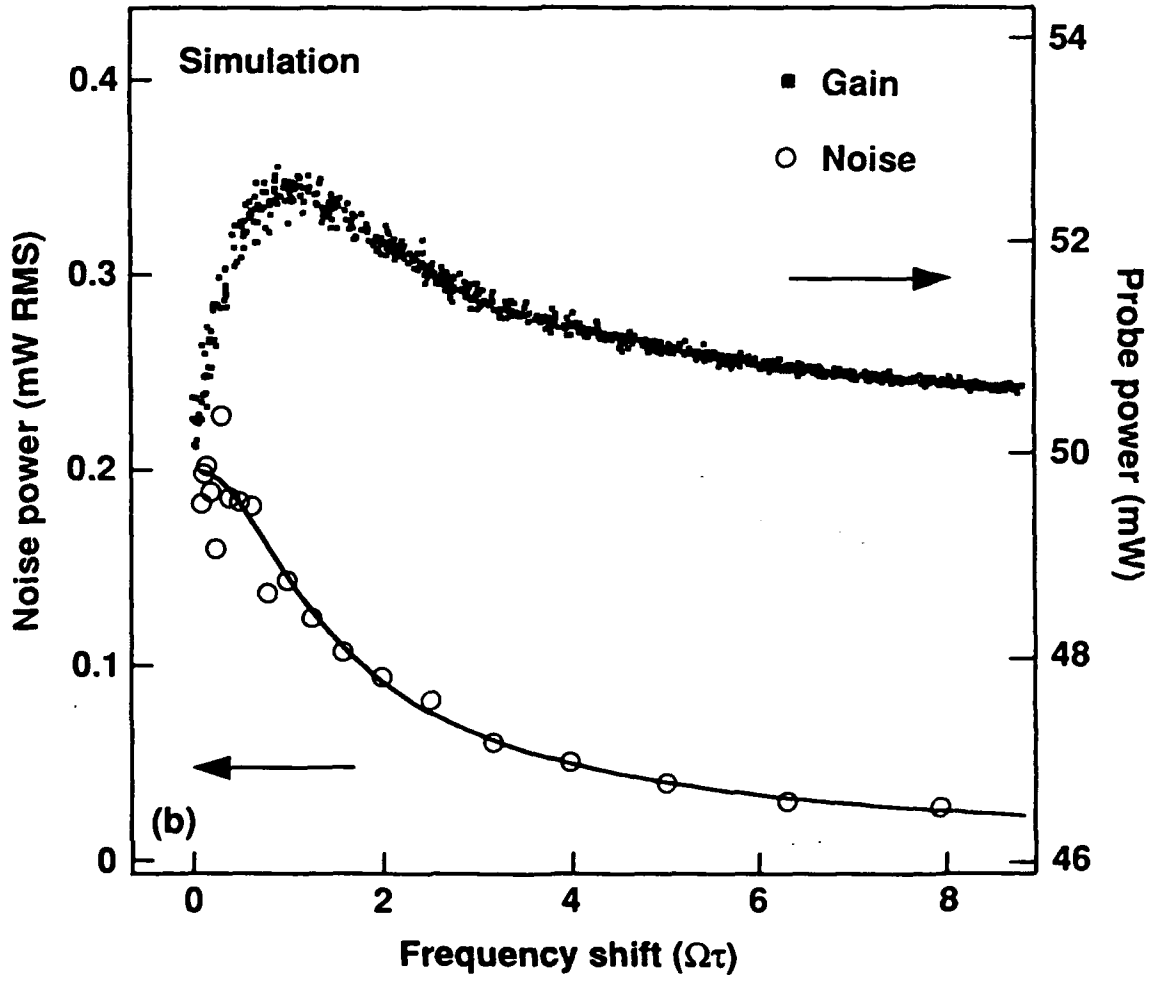
Simulation
Gain
Noise
(b)
Noise power (mW RMS)
Probe power (mW)
Frequency shift (Ωτ)
0
0.1
0.2
0.3
0.4
46
48
50
52
54
0
2
4
6
8

EXCESS NOISE INTRODUCED BY BEAM PROPAGATION THROUGH AN ATOMIC VAPOR

Martti Kauranen, Alexander L. Gaeta, William V. Davis, and Robert W. Boyd

The Institute of Optics, University of Rochester, Rochester, NY 14627

Summary

We propose and show experimental evidence of a mechanism that is important in reducing the amount of noise reduction that can be achieved at low (< 100 MHz) frequencies utilizing atomic vapors as the nonlinear medium.[1] The mechanism is based on the two-beam-coupling gain[2] experienced by the vacuum sidebands of a weak probe wave as it interacts with a strong degenerate pump wave in an atomic vapor. The mechanism leads to the amplification of intensity fluctuations of an initially shot-noise-limited probe field.

To describe this noise amplification process theoretically, we assume that the interaction between the pump and probe beams at the same carrier frequency ω_0 can be treated as a quantum-noise-limited amplifier[3] with frequency dependent gain for the probe beam and its vacuum sidebands. The power spectrum $S(\Omega)$ of the intensity fluctuations of the transmitted probe beam at a non-zero frequency Ω normalized to the shot noise level of the input can readily be shown to be given by the equation

$$S(\Omega) = |g(\omega_0)|^2 [1 + |h(\omega_0 - \Omega)|^2 + |h(\omega_0 + \Omega)|^2], \quad (1)$$

where $|g(\omega)|^2$ is the gain of the amplifier at frequency ω and $|h(\omega)|^2 = |g(\omega)|^2 - 1$ for $|g(\omega)|^2 > 1$ and $|h(\omega)|^2 = 0$ for $|g(\omega)|^2 < 1$. In the case of two-beam coupling gain that we consider, the gain at the sidebands $\omega_0 \pm \Omega$ of the probe field can be substantial and thereby lead to

dramatically increased fluctuations in the probe beam.

To study the noise properties of the transmitted probe beam experimentally, we used potassium vapor as the atomic medium (Fig. 1). The pump and probe beams were derived from a single-mode continuous-wave dye laser that was tuned close to the $4S_{1/2} \rightarrow 4P_{3/2}$ transition of potassium at the wavelength of 767 nm. The two beams intersected within a 0.5 cm long vapor cell containing potassium at a number density of 3×10^{13} cm^{-1}. The transmitted probe beam was detected with a fast photodiode, and the resulting photocurrent was amplified and spectrally analyzed.

In Fig. 2 we show the experimental and theoretical results for the rms noise voltage of the transmitted probe beam in a narrow bandwidth at 10 MHz as a function of the laser detuning from resonance. The noise spectra are normalized to the shot noise level of the input beam. For these particular measurements, the crossing angle between the pump and probe beams was 2.6 degrees and the pump intensity was ~20 W/cm^2. The theoretical curve represents the best fit to the experimental results. In Fig. 3 we show the experimental and theoretical results for the rms noise voltage as a function of spectrum analyzer frequency for the case where the laser was detuned by ~1.5 GHz to the blue from the potassium line center. The experimental conditions and the parameters used in the theoretical model are the same as in Fig. 2. The noise level falls off rapidly as a function of the spectrum analyzer frequency but exceeds the shot noise level of the input for all frequencies studied.

1. M. W. Maeda, P. Kumar, and J. H. Shapiro, J. Opt. Soc. Am. B 4, 1501 (1987).

2. M. T. Gruneisen, K. R. MacDonald, and R. W. Boyd, J. Opt. Soc. Am. B 5, 123 (1988).

3. Y. Yamamoto and H. A. Haus, Rev. Mod. Phys. 58, 1001 (1986).

Figure captions

Figure 1. A pump beam at frequency ω_0 and a degenerate probe beam with vacuum sidebands at frequencies $\omega_0 \pm \Omega$ interacting in an atomic vapor cell. The transmitted probe beam is detected, amplified, and spectrally analyzed.

Figure 2. The rms noise voltage of the transmitted probe beam in a narrow bandwidth at 10 MHz as a function of the laser detuning from resonance. The noise voltage is normalized to the shot noise level of the incoming beam. The solid line is the experimental result and the dashed line is the theoretical prediction based on Eq. 1.

Figure 3. The rms noise voltage of the transmitted probe beam as a function of spectrum analyzer frequency for the case of laser detuning from resonance of ~1.5 GHz. The voltage is normalized to the shot noise level of the incoming beam. The solid line is the experimental result and the dashed line is the theoretical prediction based on Eq. 1.

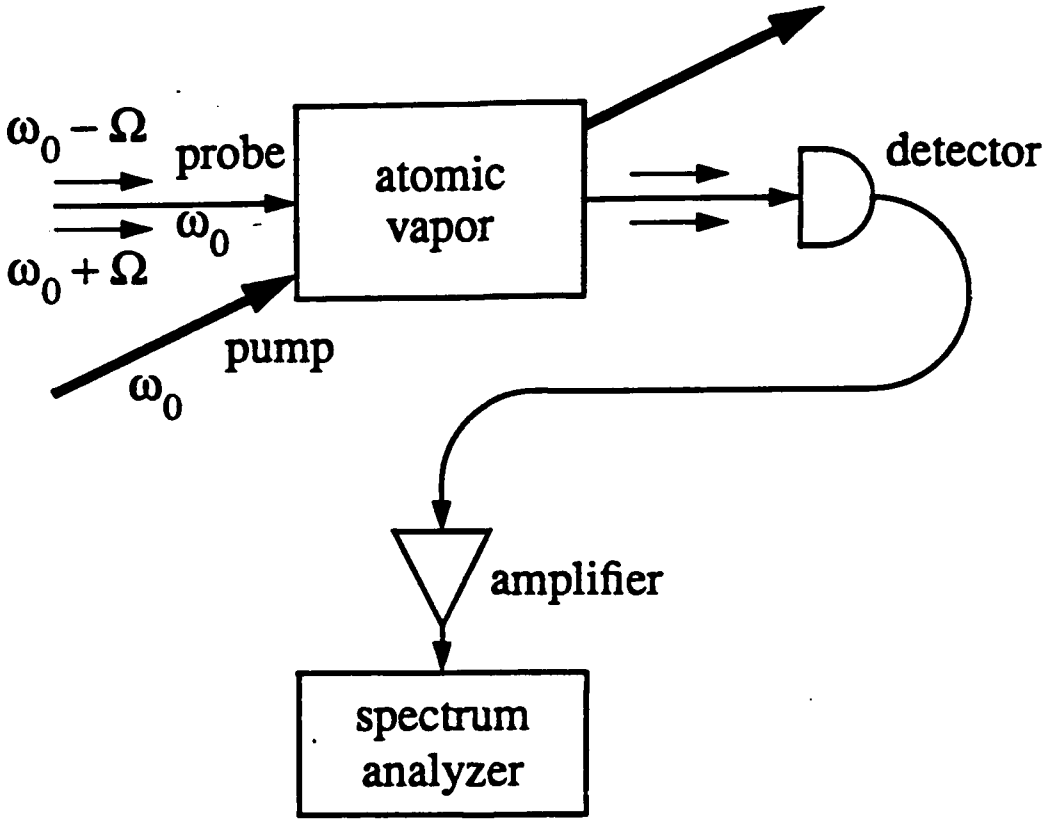

Figure 1. A pump beam at frequency ω_0 and a degenerate probe beam with vacuum sidebands at frequencies $\omega_0 \pm \Omega$ interacting in an atomic vapor cell. The transmitted probe beam is detected, amplified, and spectrally analyzed.

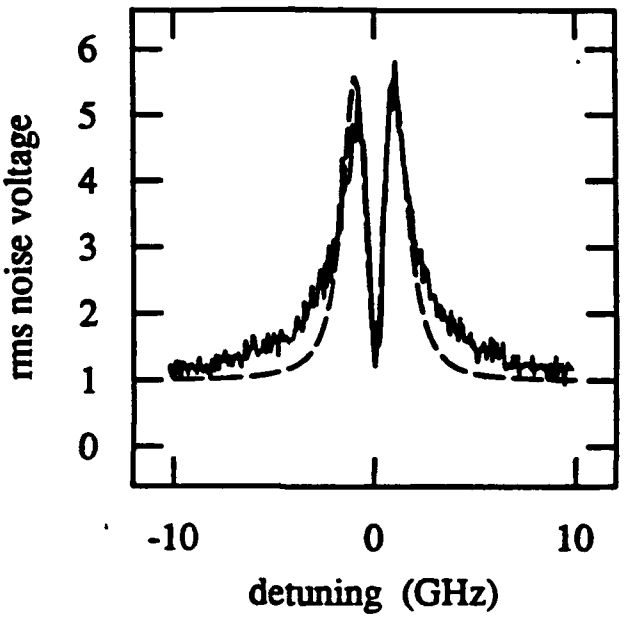

Figure 2. The rms noise voltage of the transmitted probe beam in a narrow bandwidth at 10 MHz as a function of the laser detuning from resonance. The noise voltage is normalized to the shot noise level of the incoming beam. The solid line is the experimental result and the dashed line is the theoretical prediction based on Eq. 1.

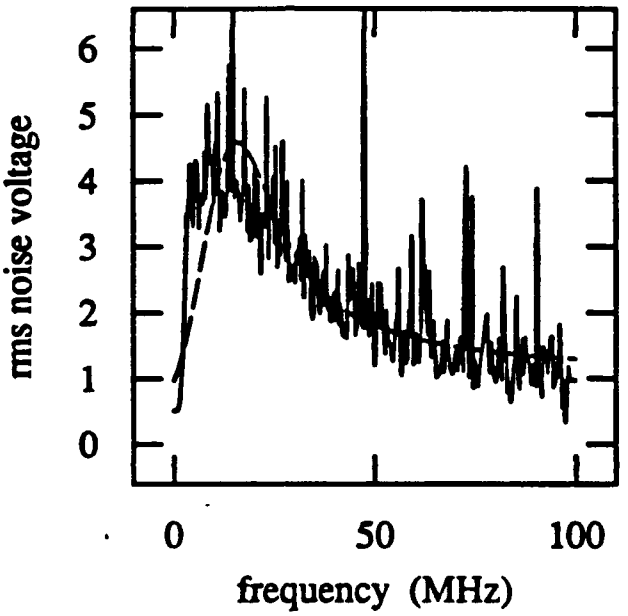

Figure 3. The rms noise voltage of the transmitted probe beam as a function of spectrum analyzer frequency for the case of laser detuning from resonance of ~1.5 GHz. The voltage is normalized to the shot noise level of the incoming beam. The solid line is the experimental result and the dashed line is the theoretical prediction based on Eq. 1.

A novel approach to all-optical switching based on second-order nonlinearities.

Gaetano Assanto, George I. Stegeman, Mansoor Sheik-Bahae, Eric VanStryland

CREOL, University of Central Florida, 12424 Research Parkway, Orlando, FL 32826

Materials with large and fast third-order nonlinearities and low losses have proven difficult to find and use in all-optical switching device configurations. Large nonlinear phase shifts, however, can be obtained in non-centrosymmetric materials relying on a cascaded second-order effect, i.e. up-conversion of a fundamental beam into its second-harmonic and the subsequent down-conversion for a phase-mismatched interaction.[1-2] Because of the recent development of efficient second harmonic generation in waveguides, it appears that phase shifts of order π can be reached over centimeter distances with peak powers of 10's of Watts or less in KTP or poled polymers, an improvement of orders of magnitude over the current capabilities of third order materials. Furthermore, this particular process exhibits several unique features which can be exploited in the realization of novel all-optical switching responses and devices which cannot be obtained with third-order nonlinearities:

1. The nonlinear phase has a steplike response with steps as large as $\pi/2$ with increasing power, exhibiting plateau's over extended ranges of excitation.
2. The fundamental at the output oscillates with input power (due to SHG) but 100% transmission can be obtained terminating the interaction at the proper length.
3. Due to the coherent nature of the interaction phase and intensity of the fundamental output can be controlled by a weak second harmonic seed.

Two structures are proposed: a bi-dimensional channel whose throughput is controlled with a second-harmonic seeding beam, and an integrated Mach-Zehnder interferometer which exhibits no pulse break-up and is formed by identical guides.

The evolution of the guided-fields propagating along a channel waveguide at the fundamental and second-harmonic frequencies can be described by:

$$\frac{d}{d\zeta} a_{2\omega}(\zeta) = -i\kappa L \cdot a^2_{\omega}(\zeta)\, e^{i\Delta\beta L\zeta} \quad (1)$$

$$\frac{d}{d\zeta} a_{\omega}(\zeta) = -i\kappa L \cdot a_{2\omega}(\zeta) \cdot a^*_{\omega}(\zeta) \cdot e^{-i\Delta\beta L\zeta} \quad (2)$$

where $|a(\zeta)|^2$ is the guided-wave power, $\zeta=z/L$ is the normalized propagation distance, L the device length, κ the effective SHG coefficient, and $\Delta\beta$ the wavevector mismatch. Due to the nature of the interaction, when $\Delta\beta\neq0$ the fundamental beam will accumulate a nonlinear phase shift related to $\Delta\beta$ and κ. Fig.1 shows a typical power and phase evolution of the fundamental versus input excitation.

We first consider the new possibilities available based on a 2ω seed beam at the input. Its phase controls the subsequent evolution of the fields along the device, even for $\Delta\beta=0$. A variety of responses can be obtained for $\Delta\beta\neq0$, different magnitudes of the seeding signals, etc. leading to phase-controlled on/off switching, phase-modulation and amplitude modulation of the strong beam at the fundamental

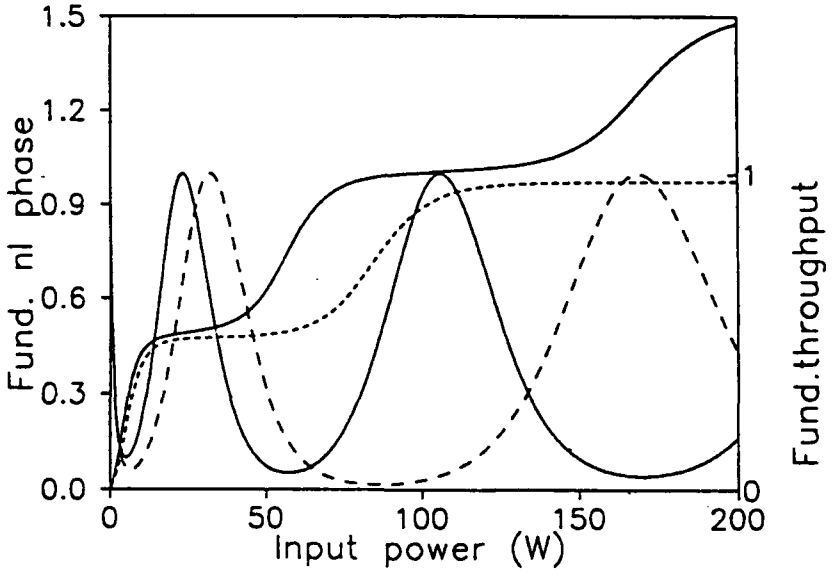

Fig.1 Throughput and nonlinear phase of a beam at frequency ω vs cw input excitation with (solid) and without (dashed lines) a seeding signal at 2ω and 180° out-of-phase. Here $\Delta\beta L=0.1$, $\kappa L=1$, and the seed is 1000 times weaker than the strong fundamental. The oscillating plots represent the throughputs, and the steplike curves represent the phase in π-units.

frequency. Fig.2a shows the throughput of the fundamental beam at the output of the channel versus the phase of the injected seed at 2ω for a phase-matched case. Note that the calculation was carried out for a seed power 1000 times smaller than the fundamental input. Fig.2b is the corresponding nonlinear phase shift imposed onto the beam at ω. The "digital" change in phase that the seed can impose onto the fundamental is apparent, with an acceptable change in throughput ($\leq$40%). This also acts as a phase amplifier near the step change in phase. In addition, note that a zero throughput is obtained for the fundamental in the absence of a seeding signal!

A straighforward configuration for utilizing the SHG nonlinear phase shift is a Mach-Zehnder interferometer shown in the inset of Fig.3. The throughput of such a device can be modulated by 100% with a relative phase change of π between the channels. Because the fundamental phase is accumulated in steps as large as $\pi/2$ (see Fig.1), if the two arms of an interferometer have opposite wavevector mismatch, the differential phase shift at the end of the guides can sum to π and allow complete switching of the fundamental beam. Such switching from on to off (or viceversa through the application of a phase bias in one arm) is particularly appealing when pulses are employed. The existence of the phase "plateau" (Fig.1) for a range of input excitations allows complete switching of most of an incoming pulse comprising

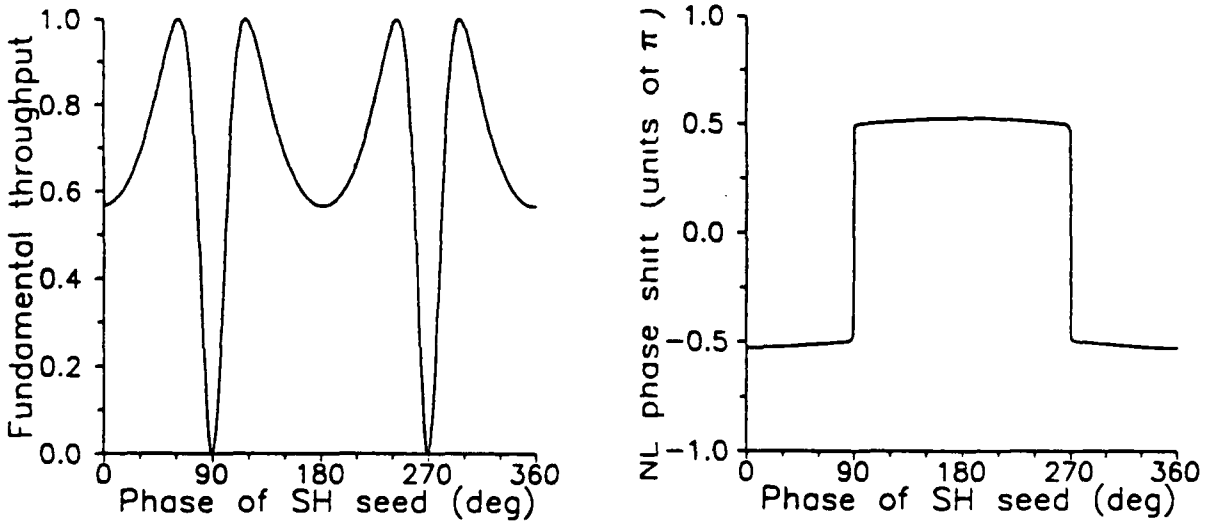

Fig.2 a) Throughput and b) phase of fundamental beam (of input power P=10W) versus the initial phase of a seeding beam at 2ω. Here $\Delta\beta L=0$, $\kappa L=2$ and the seed is 0.01W.

a distribution of peak intensities. Furthermore, under appropriate conditions, pulse narrowing will be obtained, as shown in Fig.4 for a Gaussian temporal profile. Note that similar devices based on a $\chi^{(3)}$ nonlinearity tend to exhibit pulse break-up unless solitons are employed.

In summary, a number of new all-optical switching devices can efficiently exploit the large phase shifts obtainable through cascading of a second-order process. The investigation of the response of a seeded channel and a Mach-Zehnder interferometer realized in non-centrosymmeric materials shows that some distinct advantages are offered by this approach as compared to the usual third-order phenomena. The parameters chosen for the simulation are well within reach of present-day technology, and the implementation of these concepts in KTP or $LiNbO_3$ segmented waveguides or in poled organic polymers should allow their demonstration with peak powers $\leq$100W.

1. R. DeSalvo, D.J. Hagan, M. Sheik-Bahae, G. Stegeman, E.W. VanStryland, Opt.Lett. 17, 28 (1992).
2. G.I. Stegeman, M. Sheik-Bahae, E.W. VanStryland and G. Assanto, submitted.

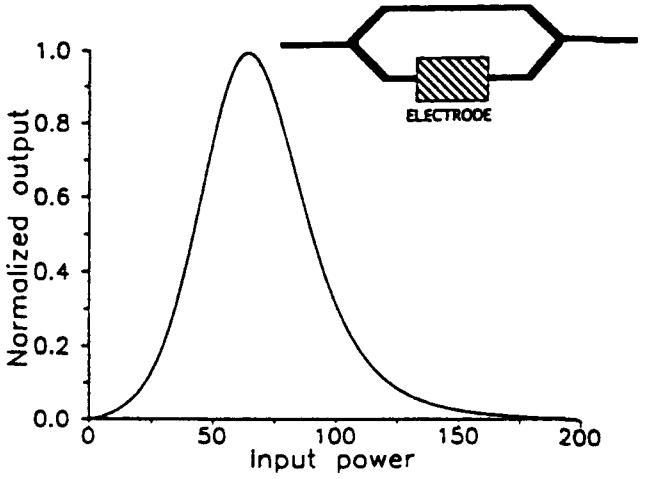

Fig.3 Response of a Mach-Zehnder interferometer (sketched in the insert) versus cw input power at ω. The device is phase-biased to provide a null output at low powers, κL=1 and ΔβL=±0.1.

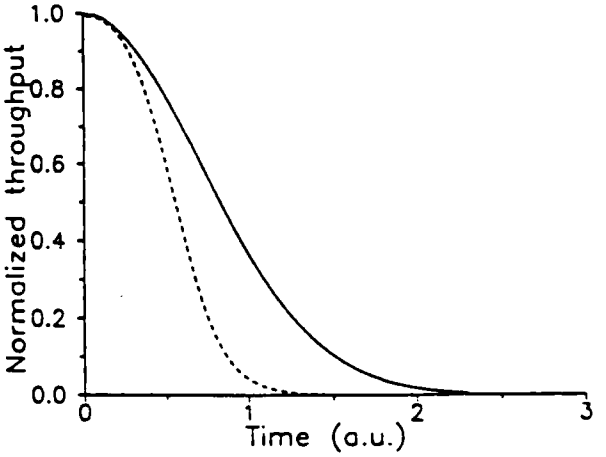

Fig.4 Response of the same Mach-Zehnder device of Fig.3 to a Gaussian distribution of input powers (solid line) versus time. Here P_{peak}=65W.

Multilayer, Nonlinear ARROW Waveguides for Surface Emitted Sum-Frequency Mixing

R. Normandin, H. Dai, S. Janz, A. Delage,
J. Brown and F. Chatenoud

Institute for Microstructural Sciences,
Solid State Optoelectronics Consortium
National Research Council
Ontario, Canada
K1A 0R6

Introduction

When used with conventional communication optical fibers, with a typical core diameter of 8μm, conventional channel waveguides geometries need to present similar thicknesses for good mode overlaps between the two. This has been a difficult goal to achieve with semiconductor waveguides due to their high index of refraction. The waveguides were typically much thinner than the fiber core and, consequently, input efficiencies were quite low. This problem was addressed some time ago with the demonstration of the antiresonant reflecting waveguide (ARROW) geometry[1]. Although these are intrinsically leaky waveguides quite acceptable losses were feasible in silicon[2] and GaAs[3] geometries. On the other hand when dealing with nonlinear interactions in semiconductor waveguides, it was realised quickly that in other to maintain acceptable overall efficiencies the waveguide thickness had to be kept unreasonably small [4]. This obviously led to input coupling difficulties. In our previous work, presented two years ago at this topical meeting [5], we demonstrated a new multilayer AlGaAs waveguide geometry with surface harmonic emission efficiencies well above what was possible in uniform films. This led to the development of several devices [6,7] such as correlators, spectrometers and intra-cavity diode laser second harmonic generators[8]. However, little attention has been given to the problem of fiber input coupling to the nonlinear waveguide. We present the first results, to our knowledge, of multi-layer core ARROW waveguides and their use in nonlinear harmonic generation. There has been little mention of the ARROW geometry in a nonlinear context, with the recent exception of inter-guide coupling[9], since they tend to be thick guiding structures.

Theory.

The general principles for the design of the ARROW structure[2,10] are well established but there is unfortunately no convenient analytical method to derive the exact modal field profile. Referring to Fig. 1, the introduction of the multilayer then precludes any easy

analytic solution for the field profile needed for the nonlinear cross section calculations. Approximations are available for both the general antiresonant conditions[2] as well as the overall losses for uniform structures[10], and these were used as the starting points for the multilayer design. To generate the mode field profile and propagation loss information, finite difference analysis[11] was performed on the multilayer system. Typically, assuming an input wavelength of 1.06μm, the multilayers were composed of alternating 80.3nm $Al_{0.9}Ga_{0.1}As$ with 72.4nm $Al_{0.65}Ga_{0.35}As$ layers. These were thus in resonance with the surface emitted 0.53μm. The first cladding was taken to be GaAs and the second cladding $Al_{0.78}Ga_{0.22}As$. The latter Al concentration gave an index of refraction consistent with the squared average permittivity of the core guide multilayers. The finite difference programme takes all the layers refractive indices and resultant reflections into account to compute the mode profiles. For example, in a 2.6μm core waveguide composed of 17 periods for the core ARROW structure the calculations yields a TE_0 mode profile as shown in Fig.2a, as well as the expected loss for both TE_0 and TM_0 vs core thickness with the same layer periodicity in Fig. 2b.

Once the exact optical field profile is known the surface harmonic emission cross-section was computed[6]. The nonlinear cross section is given by,

$$\langle S_{av} \rangle = \frac{1}{2}\Re(E_{top} \times H^{*}_{top})$$

$$= \frac{1}{2}\omega^2\sqrt{\frac{\mu_o}{\epsilon_o}}\left(\frac{n}{n+1}\right)^2 SS^{*}\ \hat{y}$$

with

$$S = \int_{-\infty}^{0} \frac{P^{nl}(y')}{n(y')} \exp\left[-ik_o \int_{-y'}^{0} n(y'')\ dy''\right] dy'$$

taking phase into account. This is shown in Fig.3. The cross section of a uniform GaAs 2.5μm thick waveguide, using our previous normalisation of a 1mm by 1cm interaction area, is of the order of 10^{-14} W^{-1} compared to 2×10^{-8} W^{-1} here, a very significant improvement.

Experimental results.

A sample with 17 periods, with the geometry previously described in Fig.1, was grown by conventional MBE methods on (100) substrates similar to GaAs based waveguides described elsewhere[6]. Light from a Nd-YAG laser at 1.06μm was coupled to the waveguide, as shown in Fig.4, by two communication fibers with a 8μm core with a 0.18

NA. Approximately 25% of the incident intensity was coupled in the guide compared with only a few percents in previous work[6,7]. Up to 15 mW average intensity (200 ns at 10kHz) was coupled in the ARROW structure. Measured propagation losses in the 4dB/cm and 8dB/cm range for TE_0 and TM_0 modes at 1.06μm were found, as predicted in Fig.2b. The interaction cross section was measured with a calibrated CCD detector and resulted in a A^{nl} of $1.76 \times 10^{-8} W^{-1}$ in close agreement with theory for a 2.6μm thick core, as shown in Fig.3. Harmonic intensities at 0.53μm of approximately 1μW were observed, almost ten times higher than previously recorded[6].

Conclusion.

Using a novel multilayer core ARROW waveguide in order to obtain high coupling efficiencies, the absolute power output of surface emitted sum-frequency generation was enhanced. This is, as far as could be determined with a literature search, the first demonstration of a multilayer core ARROW showing that the multi-reflections can be taken into account in the ARROW design and compensated by adjusting the second cladding index of refraction. Also, these are the first measurements of nonlinear harmonic generation and surface emission in ARROW type structures. Novel applications with high efficiency coupling to communication fibers, such as OTDR, DWDM and phase shift receivers and spectrometers, will be described, as well as extension to low loss double ARROWs and transverse mode control to further enhance the nonlinear cross section. Thicker samples are being grown and, due to the high modal discrimination of the ARROW structure, will result is very large coupling efficiencies in the fundamental mode for nonlinear interactions. A monolithically integrated InGaAs laser in the first cladding layer will also be discussed.

References.

1. M.A. Duguay, Y. Kokubun, T.L. Koch and L. Peiffer, Appl. Phys. Lett. 49, 13 (1986).
2. Y. Kokubun, T. Baba, T. Sakaki, Electr. Lett. 22, 892 (1986)
3. T.L. Koch, U. Koren, G.D. Boyd, P.J. Corvini, M.A. Duguay, 23, 5, 244 (1987)
4. P.J. Vella, R. Normandin, G.I. Stegeman, Appl. Phys. Lett., 38, 759 (1981)
5. R. Normandin, F. Chatenoud, R.L. Williams, NLO'90 Proceedings p228, Kauai (1990)
6. R. Normandin, S. Létourneau, F. Chatenoud, R.L. Williams, JQE-27, 1520 (1991)
7. D. Vakhshoori, S. Wang, J. Light. Tech., 9, 906 (1991)
8. H.Dai, S. Janz, R. Normandin, J. Nielsen, F. Chatenoud, R.L. Williams, accepted for publication Photonics Tech. Lett. (1992)
9. U. Trutschel, M. Mann, F. Lederer, C. Wächter, A.D. Broadman, Appl. Phys. Lett. 59, 1940 (1991)
10. T. Baba, Y. Kokubun, T. Sasaki, K. Iga, J. Light. Tech., 6, 1440 (1988)
11. K. McGreer and A. Delage, Can. 6th Semicon. Tech. Conf., Ottawa (1992)

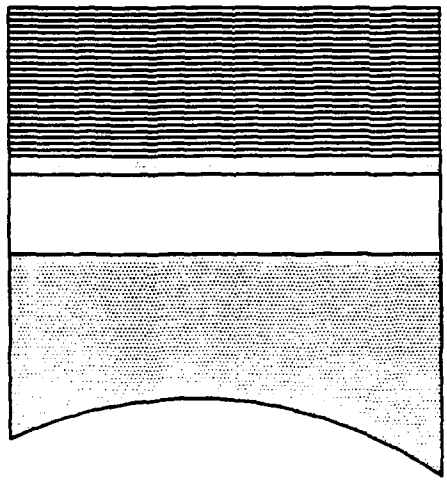

Fig. 1
Multilayer ARROW geometry

Fig. 2
(a) TE_0 mode profile for 2.6μm core
(b) ARROW attenuation

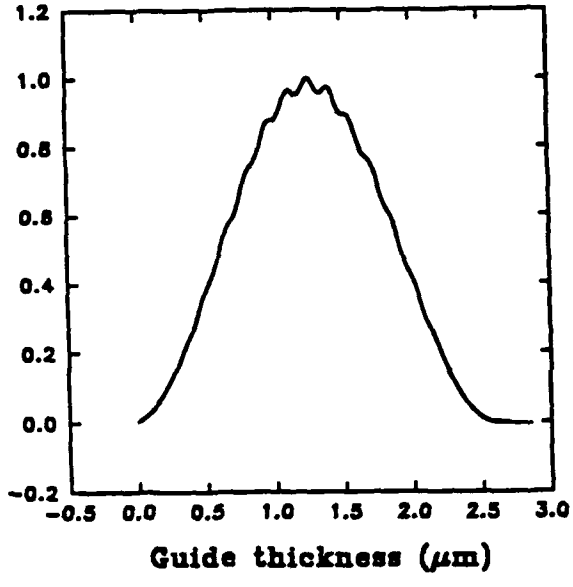

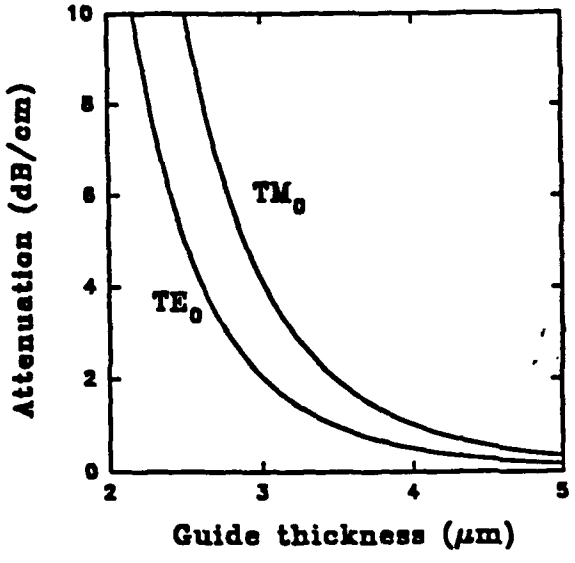

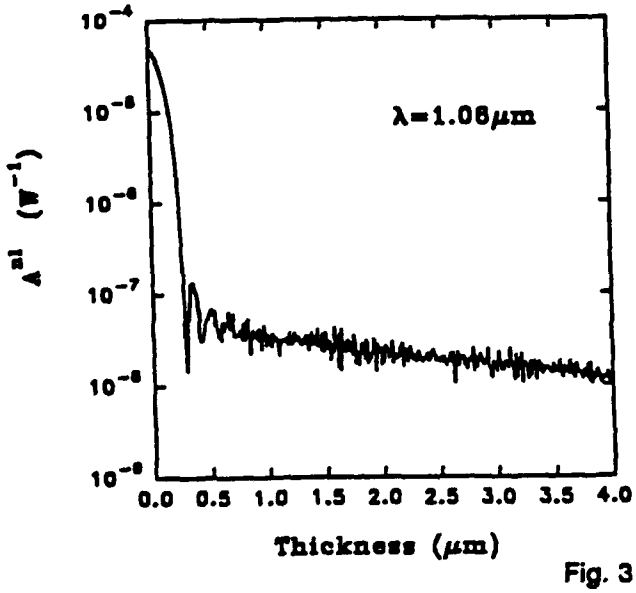

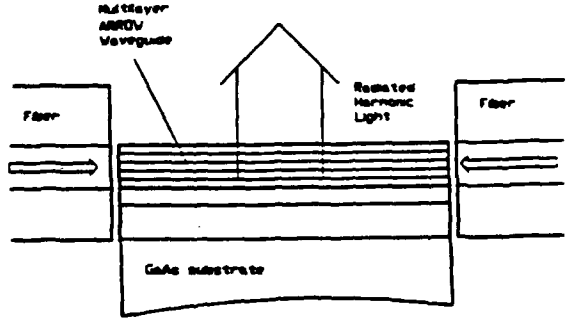

Fig.4 Measurement geometry

Fig. 3 ARROW nonlinear cross-section

ENERGY SCALING OF SBS PHASE CONJUGATE MIRRORS TO 4J

Metin S. Mangir and David A. Rockwell
Optical Physics Laboratory
Hughes Research Laboratories
Malibu, CA. 90265
(310) 317-5086

Phase conjugation (PC) via stimulated Brillouin scattering (SBS) is widely used, convenient technique for improving the performance of many pulsed lasers. For laser output energies ~1J, satisfactory performance can generally be achieved using a simple SBS phase-conjugate mirror (PCM) in which the beam to be conjugated is simply focussed into a bulk SBS medium. Exploitating PC in lasers producing output energies >10J requires a PCM that produces good conjugation fidelity at energies >1J.

The most practical approach for scaling the energy of SBS PCMs exploit a dual-cell SBS oscillator-amplifier (SBS O-A) [1]. The essential idea is analogous to master oscillator slave amplifier (MOPA) lasers. The SBS oscillator, constrained to operate at an energy level consistent with good PC fidelity, creates a weak Brillouin-shifted seed that is the conjugate of the incident pump beam. The backward-propagating seed power increases in the SBS amplifier at the expense of the incoming pump. Attenuators placed between the two cells constrain the depleted pump beam to sufficiently low intensity as it enters the SBS oscillator, which provides the required PC fidelity in this dual-cell approach. The high gain SBS amplifier produces the high reflectivity. An overdriven single-cell SBS PCM functions as an SBS O-A without the possibility of seperately controlling the amplifier and oscillator functions.

While SBS O-A have been investigated previously[2,3], this is the first report of such a device with spatially nonuniform input beam. In real world applications of PC, considerable near-field intensity variations are likely to be encountered. We find that when such collimated input beams are used in SBS O-A, it is not possible to achieve good conjugation fidelity. In particular, the output near field is highly distorted as shown in Figure 1, since the most intense parts of the input beam have a higher gain in the SBS amplifier and are preferentially reflected compared to the weaker parts.

We have overcome this limitation by spatially mixing the nonuniform input beam within the SBS amplifier. This mixing is accomplished by utilizing orthogonal pairs of cylindrical lenses on either side of the SBS amplifier cell to generate two line foci separated from one another along the propagation direction. This configuration mixes, within the SBS amplifier cell, transverse portions of the beam having different intensities. Thus the SBS gain and reflectivity become independent of the local intensity variations present at the input plane. This modification also provides high SBS gain in a physically short SBS amplifier cell while keeping the intensity on the windows

low. Note that the same mixing configuration can be used in Raman amplifiers to avoid output beam quality degredation observed when spatially nonuniform pump beams are used.

In our experiments we used the output of our Nd:glass phase-conjugate MOPA laser. It produces up to 4.5J, 35 ns FWHM pulses at 1.053 μm, and 2.5J, 25ns pulses at 0.527μm. The pump beam produces ~1.5 times diffraction limited spot at the far field, and had considerable (10:1) intensity variations at the input plane of the SBS O-A. We monitored the near- and far-field beam shapes, input and output energies, and temporal pulse shapes.

A comparison of the near field beam shapes shown in Figure 2 to the one in Figure 1 indicate the excellent near replication achieved with the SBS O-A using the spatial beam mixing method. Intensity variations with contrast ratios >10 were reproduced. We also obtained very high (0.8) far-field fidelity (defined similar to Strehl ratio) with our modified SBS A-O, as illustrated in Figure 3. In contrast, when spatially nonuniform input beams are collimated or slightly focussed within the SBS amplifier, the observed far-field fidelity was below 0.6 possibly due to near-field distortions.

The measured pulse shapes and energy reflectivity of 75% was in very good agreement with the calculated results our transient, one-dimensional computer model of the SBS A-O. We will discuss the output pulse shapes and and energy reflectivities predicted by this model as parameters such as the input pulse shape, amplifier length and SBS gain, A-O cell seperation, and acoustic decay time of the medium are varied.

We will describe the configurations and parameters that maximized the PC fidelity and energy reflectivity. We will discuss how the PC fidelity of the SBS O-A is improved at high input energies by placing appropriate attenuators between the SBS amplifier and oscillator cells. Our results are consistent with the requirement of limiting the energy reaching the SBS oscillator to less than 10-15 times its SBS threshold energy to achieve good far-field PC fidelity[4].

This work was supported by an ONR/DARPA contract.

REFERENCES

1. N.G. Basov, V.F. Efimkov, I.G. Zubarev, A.V. Kotov, and S.I. Mikhailov, "Control of the Characteristics of Reversing Mirrors in the Amplification Regime", Sov. J. Quant. Elect. 11, 1335-1337, (1981).
2. A.F. Vasil'ev and V.E. Yashin, "Stimilated Brillouin Scattering at High Values of the Excess of the Pump Energy Above the Threshold", Sov. J. Quant. Elect.. 17. 644-647. (1987).
3. G.J. Croft, M.J. Damzen, and R.A.Lamb, "Experimental and theoretical investigation of two-cell stimulated-Brillouin-scattering systems", J. Opt. Soc. Am. B8, 2282-2288, (1991).
4. J.J Ottusch, and D.A. Rockwell, "Stimulated Brillouin scattering phase conjugation fidelity fluctuations", Opt. Lett. 16,369-371,(1991).

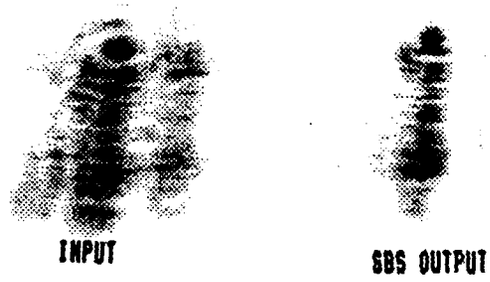

Figure 1. Near field shapes of the input and output of the SBS A-0, when a COLLIMATED beam is used within the SBS amplifier. Input energy was 1.1J at 0.527μm.

Figure 2.Near field shapes of the input and output of the SBS A-0, when SPATIAL BEAM MIXING is used within the SBS amplifier. Input energy was 4.1J at 1.053μm

Figure 3a. The far field contour plot of the input beam after a SINGLE pass through the phase aberrator (an acid etched glass plate).
Figure 3b. The far field contour plots of the input beam before passing through the aberrator and the output beam after double passing the aberrator described in Figure 3a. The far field fidelity (Strehl ratio) was 0.8. The input energy was 3.6J at 1.053 μm.

Vector Versus Scalar Theory of the Double Phase Conjugate Mirror

Kenneth D. Shaw

Nonlinear Optics Center of Technology

Phillips Laboratory

PL/LITN, Kirtland AFB, NM 87117-6008

Phone: (505)846-4750

Fax: (505)846-4651

The operation of the double phase conjugate mirror (DPCM) has in the past been described theoretically [1] through the use of one-dimensional scalar coupled wave theory [2]. This 1-d scalar theory predicts that the DPCM works as an oscillator, with the phase conjugate beams building up from zero at the crystal boundaries (as a function the longitudinal spatial coordinate) when the coupling strength is above some threshold value. In the laboratory, the DPCM does indeed appear to have this property, since its operation is observed to depend critically on the angles of the pump beams inside the crystal with respect to each other and to the crystal's optic axis, parameters upon which the coupling strength depends. The phase conjugate beams appear to "turn on" suddenly to full intensity as the orientation of the pump beams within the crystal is changed slightly.

In two recent papers [3,4], however, Zozulya et al. have shown that when the scalar theory is extended to two dimensions and different boundary conditions are applied, non-zero solutions no longer exist. That is, if the amplitudes of the phase conjugate beams are forced to be zero at their respective boundaries, they will be zero everywhere, and the

DPCM will not operate. Non-zero solutions are obtained, however, by assuming some small amount of scattering of radiation from the pump beams into the direction of the phase conjugate beams at the boundaries of the interaction region. In this case, then, there is no threshold behavior: the DPCM works for any value of coupling strength, no matter how small. A continuous variation of the phase conjugate intensity with coupling strength should be observed, and the phase conjugate intensity is proportional to the intensity of the scattered "seeds."

Up until just recently, all DPCM experiments have been performed using photorefractive crystals like barium titanate and SBN. In order to obtain the largest coupling possible, these experiments are done using radiation polarized in the plane of incidence of the pump beams (TM polarization). Strictly speaking, then, the scalar theory (either one- or two-dimensional) is not capable of describing these experiments correctly, and erroneous conclusions might possibly be drawn by so doing. By deriving the coupled wave equations directly from Maxwell's equations (as opposed to the usual derivation which starts with the wave equation), we have shown that such is indeed the case. Operation of the DPCM in cubic crystals such as BSO and indium phosphide has also been reported recently [5]. In the case of indium phosphide, TE polarization (perpendicular to the incident plane) is used. The same methods have been applied to this case also, and it has been found that there are substantial differences in the operation of the DPCM between the two situations.

Two different approaches were employed, one numerical and the other analytical. In the former approach, a numerical global minimization routine was used to determine if there are solutions to the equations which satisfy the condition that the phase conjugate

fields are zero at their respective boundaries of origin (oscillator boundary conditions). In the analytical approach, the equations are used to examine the behavior of the derivatives of the phase conjugate (PC) intensities (as opposed to the field amplitudes) at the boundaries. A necessary condition for the DPCM to operate is that the first derivative of the PC field propagating in the positive (negative) $z-$direction must be ≥ 0 (≤ 0) while the second derivatives of both PC intensities must be positive. It is found that these conditions are satisfied for TM polarization when the oscillator boundary conditions are enforced, but that in the TE case all the derivatives vanish under these boundary conditions. In this case, however, a non-zero boundary value results in the operation of the DPCM as an amplifier.

In summary, the following has been shown:

1. The double phase conjugate mirror operates as an oscillator for TM polarization and as an amplifier for TE polarization. This difference in behavior results from coupling between the transverse and longitudinal components of the electric fields which occurs in the TM case but not for TE polarization.

2. Use of the slowly varying envelope approximation leads to erroneous conclusions as far as the operation of the DPCM is concerned when the boundary conditions are applied at parallel faces of the nonlinear medium because the boundary conditions are incomplete under the SVEA. The reduction in the order of the system of differential equations that results from application of the SVEA makes it possible only to satisfy the boundary conditions on the electric field. Application of the full electromagnetic boundary conditions without making the SVEA imposes an additional constraint on

the derivative of the electric field, and it is this which changes the predictions of the theory in the TE case. That is, the boundary condition on the magnetic field cannot be neglected without leading to an erroneous result.

3. In the case of TE polarization, the use of different boundary conditions like those presented in references [3] and [4] in conjunction with the coupled wave equations derived using the SVEA leads to the same result just discussed (that the DPCM is not an oscillator) because these boundary conditions force the derivatives of the phase conjugate electric fields to vanish at the boundaries if the fields themselves vanish there.

[1] S. Weiss, S. Sternklar and B. Fischer, Opt. Lett. **12**, 114 (1987).

[2] H. Kogelnik, Bell Sys. Tech. J. **9**, 2909 (1969).

[3] A. A. Zozulya, Opt. Lett. **16**, 545 (1991).

[4] V. V. Eliseev, V. T. Tikhonchuk and A. A. Zozulya, J. Opt. Soc. Am. B **8**, 2497 (1991).

[5] N. Wolffer, P. Gravey, J. Y. Moisan, C. Laulan and J. C. Launay, Opt. Comm. **73**, 351 (1989); N. Wolffer, P. Gravey, G. Picoli and V. Vieux, OSA Technical Digest **14**, 310 (1991).

CROSSTALK AND ERROR PROBABILITY IN COUNTER-BEAM λ-MULTIPLEXED DIGITAL HOLOGRAMS

A. Yariv, Lance Glasser,
George Rakuljic, Victor Leyva

The recently proposed method for wavelength multiplexed holograms[1] raises the fundamental issues of crosstalk and error probability in such holograms. As a result we pose the following question:

A crystal with N stored λ-holograms is illuminated with, say, λ_1 in order to project out (read) hologram #1. What is the magnitude of the crosstalk field (E_N) due to reflections from the remaining N-1 holograms? Using a coupled-mode formalism[2], this field is shown to be given by

$$\frac{E_N}{E_S} = \sum_{j=2}^{N} \frac{\kappa_i}{\Delta_{j,1}} \sin\left(\Delta_{j,1} L\right) e^{i\Delta_{j,1} L} \tag{1}$$

where κ and Δ have their traditional definitions, L is the length of the crystal, $\kappa << \Delta$, and E_S is the "signal" Bragg matched field due to hologram #1. For N>>1 the central limit theorem applies and E_N can be described statistically. The resulting probability distribution is

$$p\left(E_N\right) = \frac{1}{\sqrt{2\pi\left\langle E_N^2\right\rangle}} e^{-\frac{|E_N|^2}{2\left\langle E_N^2\right\rangle}} \tag{2}$$

$$\langle E_N^2 \rangle = \frac{\pi^2}{6} \frac{\kappa^2}{\Delta^2} E_S^2 \qquad (3)$$

Equation (2) makes it possible to estimate the error probability in reading a "1" or a "0" as

$$EP = \frac{1}{2} \operatorname{erfc}[0.276\ \Delta/\kappa] \qquad (4)$$

where erfc stands for the *complimentory error function.* A plot of EP is shown in Figure 1. It is interesting to note that both the cross-talk as well as the error probability are characterized by Δ/κ. An experimental plot (Figure 2) of the reflected intensity versus λ in fixed $LiNbO_3$ holograms (N=20) shows crosstalk levels of less than -35 db compared to calculated values from (3) of ~-33 db. The corresponding error probability is $< 10^{-25}$. The relative immunity of the crosstalk to the information content is noted experimentally.

The talk will provide the detailed derivations and discussion leading to the results quoted above.

References:

(1) G. A. Rakuljic, Amnon Yariv, and V. Leyva, "High Resolution Volume Holography Using Orthogonal Data Storage." Paper MD3, Optical Society of America Topical Meeting on "Photorefractive Materials Effects and Devices," Beverly, Massachusetts 1991.

(2) Amnon Yariv, Optical Electronics, Holt, Rinehart and Winston, Phil. 1991, P. 503.

Figure 1

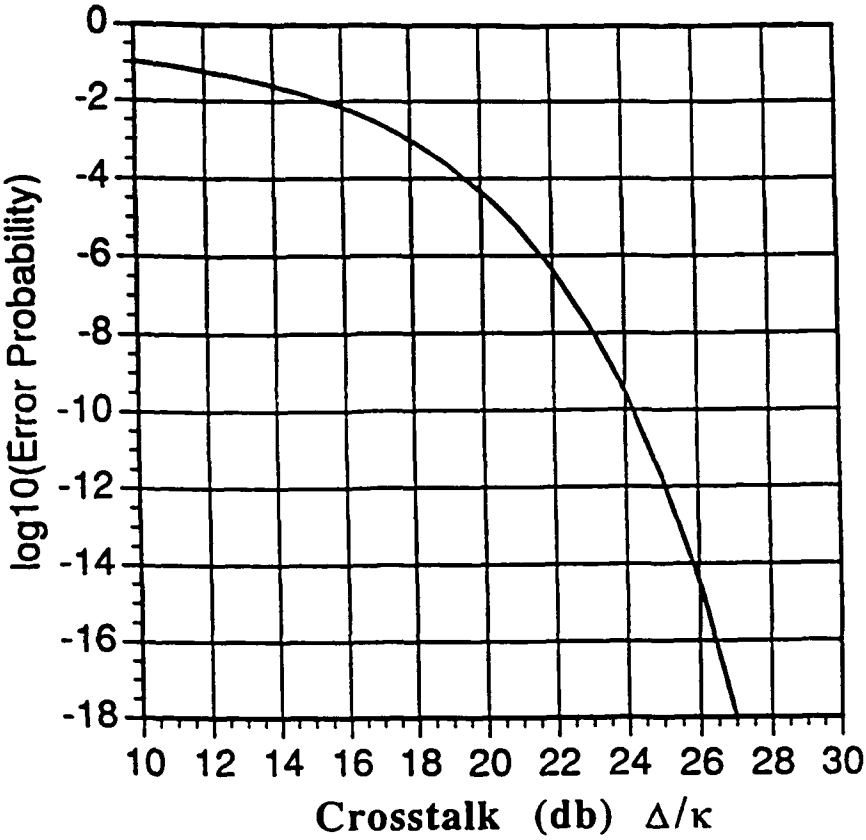

Figure 2

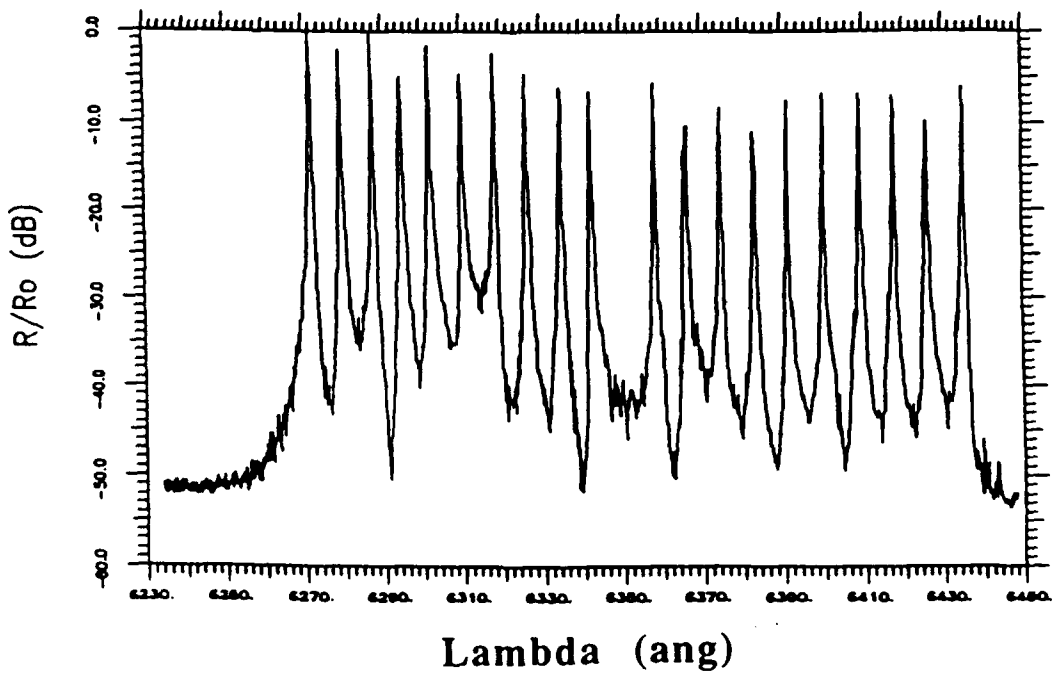

MODAL GROWTH OF SHG IN DOPED SILICA THIN FILM WAVEGUIDES

W. Roc White
Department of Physics
USAF Academy, CO 80840-5000

John J. Kester
Skip C. Pribyl
Frank J. Seiler Research Laboratory
USAF Academy, CO 80840-6528

Frequency doubling of 1064 nm laser light is observed in Ge-doped SiO_2 thin film waveguides. SHG growth is examined as a function of input polarization and waveguiding modes.

Second harmonic generation (SHG) has been observed in optical fibers once prepared with the fundamental frequency, ω,[1] or the fundamental together with a seed second harmonic, 2ω.[2] During the preparation process the SHG signal experiences a nonlinear growth until saturation.[1,3] While not well understood, the mechanism is generally attributed to a spatially varying DC field (grating) related to dopants and defects within the silica fibers,[4,5] resulting in an effective χ^2 and quasi-phase matching.[6,7] Attempts to model the interaction between the light and the fiber [8] have been hampered by the cylindrical geometry; however, the observation of SHG in planar waveguides of doped silica[9] offers further insights.

This paper examines the growth of SHG light produced in two-dimensional silica waveguides with a composition similar to optical fibers. The films are optically processed with various propagation modes of both the ω and seed 2ω light. The growth of the SHG is highly dependent on the input polarization. Additionally, observations consistent with grating evolution and subsequent erasure are presented.

Figure 1 illustrates the experimental arrangement. 1064 nm light from a Q-switched (1.22kHz) and modelocked (76 MHz) Nd: YAG laser passes through a KTP crystal producing the seed 532 nm light. The half wave plate controls the polarization of both beams. A beamsplitting mirror separates the ω and 2ω light which then passes through polarizers and filters, before being recombined. The purpose of separating the beams is to allow input coupling of the ω and 2ω light at different angles, thus different propagation modes. Care is taken to equalize the optical path length between the two branches. Both beams are then

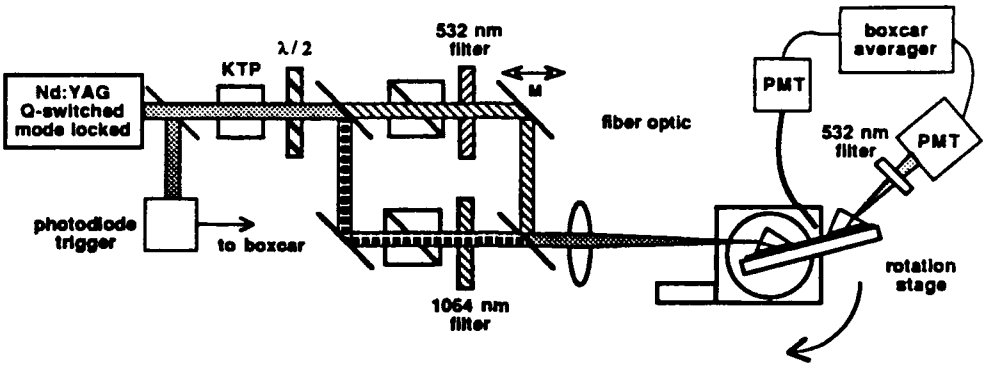

Figure 1. Experimental Setup.

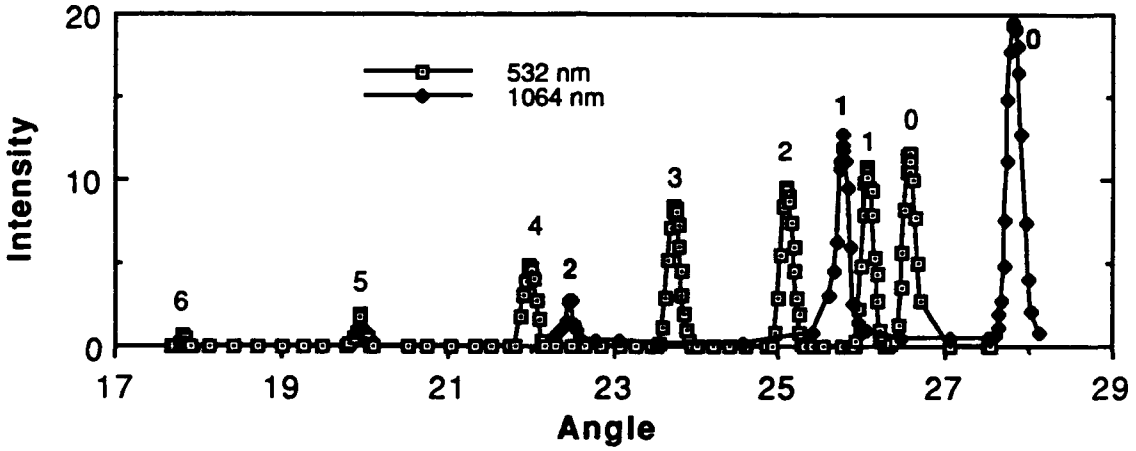

Figure 2. Waveguiding as a function of external coupling angles for 532nm and 1064 nm light. TM mode numbers are indicated.

focused onto the prism-film interface. Typical average powers for the ω and 2ω incident light are 400 mw and 1.5 mw, respectively. During measurements of the film generated SHG, the 2ω seed beam is blocked momentarily.

The thin films were produced by ion beam sputtering of silica and germanium onto optical grade fused silica substrates. Film thicknesses ranged from 1.7 to 3.6 μm, and the average surface roughness for each film was 1.5 nm. The films contained about six atomic percent germanium which was substantially oxidized.

Waveguiding in specific modes was accomplished by rotating the film and coupling prism. Figure 2 shows coupled p-polarized light intensity into a 3.6 μm film as a function of incidence angle on the prism for both the ω and 2ω light. The indices of refraction for the ω and 2ω modes were determined[10] to be 1.5315 and 1.5469. Scattering loss in the waveguide was approximately 3 db/cm for 532 nm light.

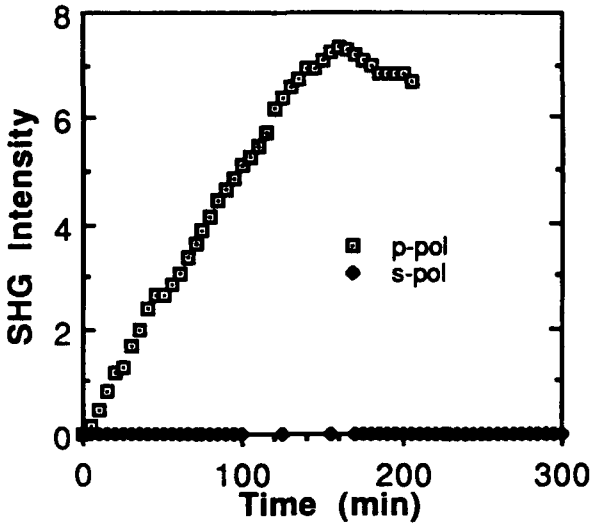

Figure 3. SHG Growth for both p and s polarizations.

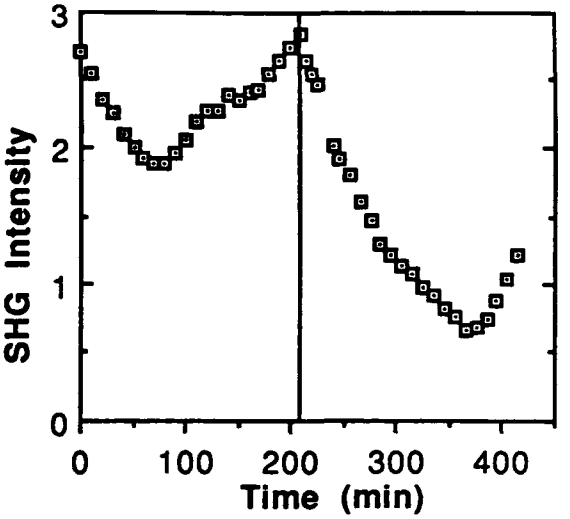

Figure 4. Grating erasure. Relative phase shifts at time 0 and 210 min.

Specific propagation modes of the 1064 nm and 532 nm light were matched by translating mirror M. Several paths within the film were prepared with different combinations of ω and 2ω modes. In each case film generated SHG grew initially with a quadratic dependence, then continued with near linear growth for several hours until saturation (Fig. 3). The generated SHG was in the same propagation mode as the seed 2ω light. Additionally, significant SHG occurred only with p-polarized input light, and the SHG was also p-polarized.

The initial growth rate of the SHG was directly related to the relative intensity of the seed 2ω beam. Stronger seed signals resulted in faster SHG growth; however, saturation levels appeared to depend more on the specific propagation modes of the ω and SHG light. Higher saturation levels were achieved for SHG modes which corresponded to 2ω modes with closer coupling angles to the fundamental, as in Figure 2. For example, the saturation level for the zeroth order SHG from the zeroth order ω was higher than that achieved when seeding with the first order 2ω. This held even if the initial SHG growth rate was smaller due to a weaker seed beam. A curious observation noted in each experiment was a significant increase in the overall throughput of both the ω and 2ω seed beams after preparation. The IR signal increased on average by 20% and the green seed signal doubled.

During many of the film preparation experiments, severe oscillations in the SHG signal over time were observed. Some of these reduced the SHG to virtually zero, even after hours of preparation time. This could be attributed to changes in the relative phase between the ω and 2ω seed beam.[5] Figure 4 shows oscillations induced in the SHG by placement of a

neutral density filter in the 532 nm branch after saturation (at reference time zero), thereby causing a random phase shift in the seed beam relative to the 1064 nm beam. The SHG signal immediately decreased then after roughly an hour began to increase again. At 210 minutes, the filter was removed, resulting in another phase shift and a repeat of the SHG oscillation. This behavior could be attributed to the formation, erasure, and reformation of index gratings within the film.

The growth of SHG in amorphous thin films we have observed is comparable to that observed in optical fibers of similar composition. The geometry of the two dimensional thin film waveguides enables greater control of the conditions for SHG growth. The results to date are consistent with models for the development of index gratings within the waveguides. The difference in SHG produced in the p versus the s polarizations could be due to more effective trapping of ejected electrons[11] along the film-substrate interface. The observation of oscillations in the SHG due to induced phase changes between the ω and 2ω beams suggest formation and erasure of these gratings. Further studies examining the effect of propagation modes and intensities on the SHG are warranted.

REFERENCES

1. U. Osterberg and W. Margulis, Opt. Lett., **11**(8), 516 (1986).
2. R. H. Stolen and H. W. K. Tom, Opt. Lett., **12**, 585 (1987).
3. A. Krotkus and W. Margulis, App. Phy. Lett., **52**(23), 1942 (1988).
4. D. Z. Anderson, V. Mizrahi, and J. Sipe, Opt. Lett., **16**(11), 796 (1991).
5. B. Ehrlich-Holl, D. M. Krol, R. H. Stolen, and H. W. K. Tom, Opt. Lett., **17**(6), 396 (1992).
6. R. H. Stolen, **Nonlinear Waves in Solid State Physics**, edited by A. D. Boardman, et. al., Plenum Press, New York (1990).
7. A. Okada, K. Ishii, K. Mito, and K. Sasaki, Applied Phys. Lett., **60**(23), 2853 (1992).
8. U. Osterberg, R. I. Lawconnell, L. A. Brambami, C. G. Askins, and E. J. Friebele, Opt. Lett., **16**(3), 132 (1991).
9. J. J. Kester, P. J. Wolf, and W. R. White, Opt. Lett. (accepted for publication).
10. R. Ulrich and R. Torge. App. Opt., **12**, 2901 (1973).
11. N. B. Baranova, A. N. Chudinov, A. A. Shulginov, and B. Ya. Zel'dovich, Opt. Lett., **16**(17), 1346 (1991).

KEY TO AUTHORS